

40
1/21/94 [Signature]

PREPARED FOR THE U.S. DEPARTMENT OF ENERGY,
UNDER CONTRACT DE-AC02-76-CHO-3073

PPPL-2959
UC-420

PPPL-2959

NONLINEAR COUPLING OF LOW- n MODES IN PBX-M

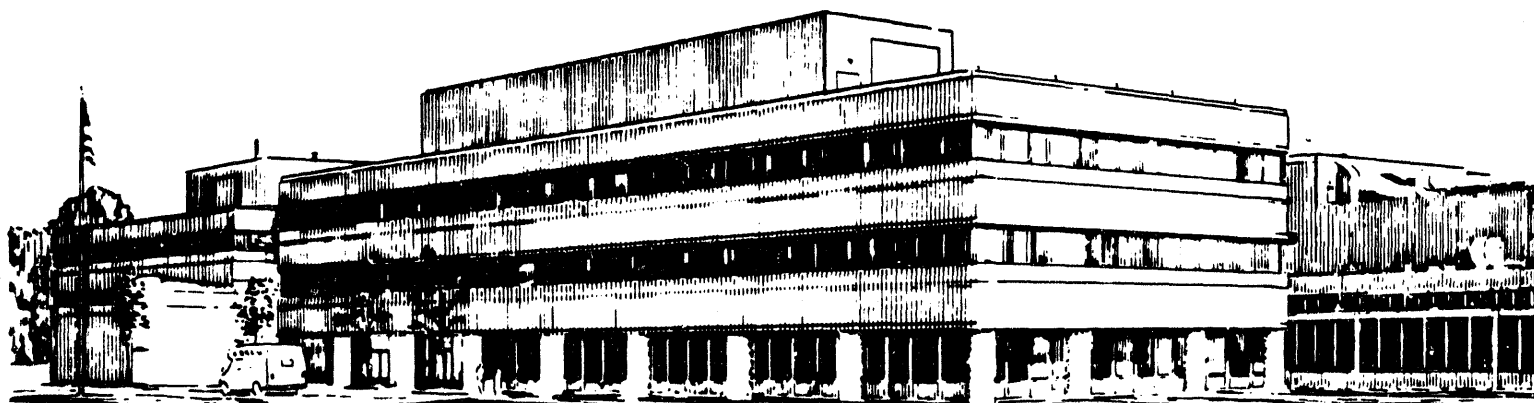
BY

S. SESNIC, R. KAITA, S. KAYE, ET AL.

MARCH, 1994

PPPL

PRINCETON
PLASMA PHYSICS
LABORATORY



DISTRIBUTION OF THIS DOCUMENT IS UNLIMITED

NOTICE

This report was prepared as an account of work sponsored by an agency of the United States Government. Neither the United States Government nor any agency thereof, nor any of their employees, makes any warranty, express or implied, or assumes any legal liability or responsibility for the accuracy, completeness, or usefulness of any information, apparatus, product, or process disclosed, or represents that its use would not infringe privately owned rights. Reference herein to any specific commercial produce, process, or service by trade name, trademark, manufacturer, or otherwise, does not necessarily constitute or imply its endorsement, recommendation, or favoring by the United States Government or any agency thereof. The views and opinions of authors expressed herein do not necessarily state or reflect those of the United States Government or any agency thereof.

NOTICE

This report has been reproduced from the best available copy.
Available in paper copy and microfiche.

Number of pages in this report: 38

DOE and DOE contractors can obtain copies of this report from:

Office of Scientific and Technical Information
P.O. Box 62
Oak Ridge, TN 37831;
(615) 576-8401.

This report is publicly available from the:

National Technical Information Service
Department of Commerce
5285 Port Royal Road
Springfield, Virginia 22161
(703) 487-4650

NONLINEAR COUPLING OF LOW- n MODES IN PBX-M

S. SESNIC, R. KAITA, S. KAYE, M. OKABAYASHI, R.E. BELL, G.M. GAMMEL^(a),
A. HOLLAND^(b), H.W. KUGEL, B. LEBLANC, F.M. LEVINTON^(c), and H.
TAKAHASHI

Princeton Plasma Physics Laboratory, Princeton University
P.O. Box 451
Princeton, New Jersey, 08543
USA

and

E.J. POWERS and SUNGBIN IM

Department of Electrical and Computer Engineering, The University of Texas at Austin
Austin, Texas 78712-1084
USA

ABSTRACT

In many of the medium and high beta discharges in PBX-M low- n modes with different n -numbers are observed. The probability of a low- n mode to be excited decreases with increasing n -number. If two modes of different frequency and n -number (ω_1 and ω_2 ; k_1 and k_2) are simultaneously present in the plasma, these modes interact nonlinearly and create sidebands in frequency ($\omega_2 \pm \omega_1$) and wave-number ($k_2 \pm k_1$ or $n_2 \pm n_1$ and $m_2 \pm m_1$). If these fundamental modes, ω_1/k_1 and ω_2/k_2 , contain strong harmonics, the harmonics also interact nonlinearly, creating more nonlinear products: $k\omega_2 \pm l\omega_1$ and $kk_2 \pm lk_1$, where k and l are integers describing the harmonics. These modes, the products of nonlinear interaction between two fundamental modes, most probably have a kink character. During this three-wave coupling interaction, a decrease in neutron rate and an enhanced loss of medium energy ions are observed.

MASTER

DISTRIBUTION OF THIS DOCUMENT IS UNLIMITED

EB

1. INTRODUCTION

Understanding and controlling high- β plasma operation are among the more important issues, for a fusion reactor if it is to become economically-viable future source of energy. The main purpose of PBX-M experiments is to develop a scenario for stable high- β operation by achieving and exploring the second regime of stability against ideal ballooning modes, and by developing preventive measures against external kinks. To achieve this goal, two scenarios were developed. In the first scenario, a fast current ramp (up to 2.4 MA/sec) was applied to obtain a broad current profile and a large ratio of plasma current to the product of the minor radius and the toroidal magnetic field ($I/aB=2.1$ MA/m-T). Using this scenario, a high volume-averaged toroidal beta, $\langle\beta_t\rangle$, was obtained with values of up to 6.8%. [1,2] The second scenario was to approach the second stability regime by operating at high values of a maximum normalized beta, $\langle\beta_n\rangle=\langle\beta_t\rangle/(I/aB)$, or high values of poloidal beta, $\beta_{pol}=8W_{tot}/(3\mu_oR_oI_p^2)$. In this scenario, with a moderate I/aB of 0.9 MA/m-T, a β_{pol} of 2.4 and β_n of 4.5 were obtained.

This paper is concerned with the nonlinear interaction between low- n MHD modes observed during the experiments at high- β_{pol} on PBX-M. The first observations of this nonlinear interaction were made on PBX-M and were reported in 1991. [3] It was observed that two independent low- n modes of two different n -numbers interacted nonlinearly, creating two sidebands characterized by the sum and difference in frequency and n -numbers. Experimental findings of a similar three-wave non-linear coupling of spatial Fourier modes in the MST reversed field pinch experiment were later reported by the University of Wisconsin group. [4] Using the bicoherence method, [5] the authors investigated poloidal and toroidal three-wave coupling of modes of different m - and n -numbers. They showed that the bicoherence in the poloidal direction (m -numbers) displays only two peaks, while the bicoherence in the toroidal direction involves many toroidal modes. They also reported good agreement between the experimental data and initial value resistive MHD code calculations. The PBX-M group reported on a different phenomenon: the very strong nonlinear interaction between a low frequency, low- n ($m=1/n=1$) MHD mode and a high frequency, high- m and - n ($m=6\pm 1/n=5\pm 1$; possibly TAE) mode. [6]

These low frequency, low- n nonlinear mode interactions were observed in PBX-M under several different plasma conditions. The plasma current was varied between 200 and 350 kA and the neutral beam injection between 2 and 5 MW. The toroidal field was approximately 1.3 T and average densities were above 3×10^{13} cm⁻³. The electron and ion temperatures varied

from above 1 to 2 keV, elongation between 1.5 and 1.9, and indentation between 15% and 18%. The triangularity was 0.3. The range of toroidal beta was 0.8 to 3.5 %. The nonlinear interaction was observed under all of these conditions, indicating that this three-wave coupling is not only a high- β effect.

The principal diagnostics used to obtain data on the nonlinear mode interaction were the soft x-ray diode array, poloidal and toroidal magnetic probe arrays, energy resolved charge-exchange flux measurement, neutron rate detector, neutral probe beam, and motional Stark effect (MSE) polarimetry to measure q-profiles.[7, 8, 9] The lines-of-sight of the soft x-ray diode array are shown superimposed on the flux surfaces in Fig. 1. The vertical distance between the midplane and the intersection between the line-of-sight and the vertical at $R_0=165$ cm defines the radial profile dimension z used in the paper.

The present work establishes that the nonlinear interaction of two independent low- n modes results in weak turbulence that possibly introduces a further deterioration of energy confinement.

The experimental results are described in the second section. First, the solitary low- n modes are described. The second part of the second section is devoted to the interaction of two fundamental modes. It is shown that this interaction occurs for a wide variety of low- n -numbers. The importance of the interaction of higher harmonics is also demonstrated, especially in the case of an enhanced mixing during the sawtooth precursor and sawtooth crash. In Section Three, the fast ion losses during this nonlinear interaction are described, indicating an enhanced fast ion loss during this weak turbulence period. Finally, in Section Four, the discussion of the significance of the nonlinear mode interaction on the enhanced plasma losses is presented.

2. EXPERIMENTAL OBSERVATION

A low- n MHD mode is excited at a given rational surface if the instability conditions for the mode on that magnetic surface are satisfied. Because of the toroidal coupling this mode will cause the growth of secondary modes on other magnetic surfaces. These secondary modes satisfy the conditions that they have the same toroidal n -number and that the m -numbers of the secondary modes are given by $m_s = m_p \pm l$, where m_p and m_s are the primary and secondary poloidal mode numbers and 'l' is an integer. They, therefore, reside on the magnetic surfaces given by $q = (m_p \pm l)/n$. Usually this mode is the dominant mode and no other mode of a different n -number is present.

This is, however, not always so: sometimes the condition for instability is satisfied

simultaneously on two rational surfaces and for two different toroidal mode numbers n_1 and n_2 . In this case, either the primary mode or the secondary modes with the toroidal mode number n_2 can be excited on or near the same magnetic surfaces already occupied by the other mode with different toroidal mode number n_1 . If this happens, the two modes will interact, and this interaction will be nonlinear. This means that the two different modes are not superimposed on each other by simple local addition, but that their interaction has a nonlinear, quadratic character. This kind of interaction will create new modes (sidebands), such that the frequencies, ω , and the wavenumbers, \mathbf{k} , satisfy the selection rules for three-wave interaction: $\omega_{3,4} = \omega_1 \pm \omega_2$ and $\mathbf{k}_{3,4} = \mathbf{k}_1 \pm \mathbf{k}_2$. This non-linear interaction is the cause of the weak turbulence.

2.1 Characteristics of low-n modes

Before discussing the experimental evidence for the three-wave interaction, the modes, which are almost always observed to interact with each other, will be described, and their amplitude profiles, as observed by the soft x-ray diode array, will be shown. These are the modes with the toroidal mode numbers $n=1$ to 4. These modes were mostly observed after the β -collapse in high- β_{pol} discharges, and during the time of a strong edge activity (giant ELM's and small ELM-like events in H-mode plasmas). [1, 10] They are discussed in the following in order to clarify the more complicated cases of nonlinear interaction between these modes. The soft x-ray profiles of these low-n modes are shown in Figs. 2 and 3 for various n-numbers. These figures show three profiles: the amplitude profile, $S_x(z)$, the normalized amplitude profile, $S_x(z)/S_0(z)$, and the phase profile, $\phi(z)$. $S_x(z)$ is the fluctuation power integrated over the narrow bandwidth of the mode ($\approx 3\text{kHz}$), $S_0(z)$ is the D.C. component of the soft x-ray signal, and $\phi(z)$ is the phase difference between the fluctuation signal of the central diode ($z=0$) and the fluctuation signal of a diode at any other position z . Because the soft x-ray signals represent line-of-sight integrated intensities, it is important to know both the normalized fluctuation amplitude, $S_x(z)/S_0(z)$, as well as its absolute value, $S_x(z)$. The normalized fluctuating amplitude is the key quantity, but the profile of the absolute amplitude is necessary to localize the mode spatially. The displacement vector, $\xi = S_x^{1/2}/[\text{grad}(S_0^{1/2})]$, is not shown in the figures, but in the central part of the plasma (at the $q=1$ and between $q=1$ and $q=2$ surfaces), its form is not very different from the normalized power spectrum.

The spectral profiles of the photon noise (denoted by Ph in the figures) are calculated using the expression $S_{v,\text{noise}} = (2S_0 \langle E_v \rangle \Delta f)^{1/2}$, where S_0 is the average soft x-ray power falling on the diode in Watts, $\langle E_v \rangle$ is the average photon energy seen by the diode,

determined by the plasma temperature and by the material and thickness of the soft x-ray filter in front of the diode, and Δf is the frequency bandwidth determined by the spectral width of the Fourier analysis.

In the Fig. 2 are shown two cases of an $n=1$ mode with an observed central $m=1/n=1$ component. In the first case, a small $m=1/n=1$ island causes a weak relative fluctuation amplitude of 3%, with a correspondingly small island width of less than 5 mm (Fig. 2a). In the second case, a large $m=1/n=1$ island with an island width of 3.5 cm results in a relative fluctuation amplitude of 20% (Fig. 2b). Although the poloidal and toroidal β 's in the two cases are comparable, the small island case does not show observable "ballooning", whereas the large island case shows a strong "ballooning" character.[6] The two examples give rise to different types of nonlinear interaction in the presence of an additional independent mode in the plasma. The "ballooning" character of the large $m=1/n=1$ island is obviously an effect of the size of the island, but it is not understood. The behavior of the phase profile is also different for the two cases. The small island case has, as expected, a symmetric up/down profile (slope) with a central jump of $\sim 160^\circ$. The large island case shows a slower change in phase and a strong up/down asymmetry in the slope, which reflects up-down asymmetry in the poloidal (and toroidal) phase velocity. One possible reason for the "ballooning" character and the up-down phase asymmetry of the large $n=1$ mode might lie in a combination of a strong perturbation in the Shafranov shift due to the large non-axisymmetry, and toroidal and poloidal rotation effects. In the case of a strong island, the strongest relative fluctuation (Fig. 2b) occurs around $z=50$ cm. This is the location of the $m=3/n=1$ perturbation. It seems that the driving mode is the $m=3/n=1$ mode, as opposed to the situation with the small $m=1/n=1$ island (Case a), where the driving mode resides on the $q=1$ surface ($m=1/n=1$ mode). This is also reflected in the lower frequency: the large amplitude mode frequency is about 7 kHz and the small amplitude mode has a frequency of 15 kHz. The probable reason for the difference in frequency lies in the different toroidal or poloidal rotation velocities of the plasma at $q=1$ (small $m=1/n=1$ island case) and $q=3$ (large $m=1/n=1$ island case) surfaces.

The other two examples show a strong $2/2$ or $3/3$ mode on the $q=1$ surface (Figs. 3a and 3b) and another component of the mode outside the $q=1$ surface. The $n=4$ mode is not shown. Some of the parameters of these modes are given in Table I. The frequency of the mode increases roughly linearly with the n -number. The position of the mode outside the $q=1$ surface ($z \approx 25$ cm) is described by the position of the mode maximum and successive minimum, z_{\max} and z_{\min} . Both of these positions move inward with the increasing n -number, indicating that these modes are most probably $3/2$, $4/3$, and $5/4$ modes. From the normalized amplitudes of these modes, S_f/S_0 , at $z_{\max} \approx 33, 30,$ and 27 cm, corresponding to the $2/2, 3/3,$

and 4/4 modes on the $q=1$ surface (Figs. 4b to 6b), one can speculate that these modes (3/2, 4/3, and 5/4) must be the driving modes. The modes on the $q=1$ surface (2/2, 3/3, and 4/4) were created by toroidal coupling. Note that all of these modes saturated at relative amplitudes between 2% and 3%, which would indicate that the islands are relatively small with the island width less than 1 cm.

The time averaged values of the soft x-ray intensity profiles for these modes show a strong similarity in the central part of the plasma ($|z| \leq 25$ cm), but they differ in the region $45 \text{ cm} \geq |z| \geq 25$ cm. This should indicate that there is a difference in the current and pressure profiles and their gradients in the region, where these modes are excited ($q=1, 3/2, 4/3, 5/4$). Although the profiles and gradients are changed by these modes, this difference in the soft x-ray profiles must itself be an indication that the current and/or pressure profiles and their gradients play a role in exciting these modes. The slight differences in the gradients in the region between $q=1$ and 2 is most probably the reason that at different times, different m/n modes are excited.

The last line in Table I shows how many times a particular n -number was observed in 17 discharges. The most often observed was the $n=1$ mode, which was observed 11 times (probability of over 60%). The probability of exciting an $n=2$ mode was somewhat lower, about 40% (7 times), of $n=3$ about 20%, and $n=4$ occurred only once. The sum of the probabilities is larger than one, because in some discharges more than one mode was observed.

2.2 Phenomenon of Low- n Weak Turbulence

Nonlinear coupling of two modes of frequencies ω_1 and ω_2 , and wave numbers k_1 and k_2 , is characterized by the presence of at least two additional perturbation components that satisfy the following expressions for frequency and wave number: $\omega_2 \pm \omega_1$ and $k_2 \pm k_1$. This nonlinear interaction occurs because the plasma is a nonlinear medium that not only transports the waves but also causes them to interact. From the wave number expression, the same selection rule of subtraction/addition will apply to the toroidal and poloidal mode numbers, n and m , so that the additional perturbations will have toroidal and poloidal mode numbers: $n_2 \pm n_1$ and $m_2 \pm m_1$, respectively. The n -number is determined from a toroidal array of magnetic probes. To establish the m -number is more difficult because of the complex shape of the PBX-M plasma, and because many of the magnetic probes of the poloidal array were placed too far from the plasma surface to yield complete poloidal information. However, the poloidal m -number in the central part of the plasma could be established from the mode fluctuation

profile using the soft x-ray diode array.

One example of the nonlinear wave coupling between the $n=1$ and $n=3$ modes is shown in Figs. 4 to 8. Fig. 4 shows the soft x-ray signals for different radial positions in the plasma and the Mirnov probe raw data. The signals in the central part of the plasma ($|z| \leq 10$ cm) are dominated by the lower frequency $n=1$ mode, and in the outer region ($|z| \geq 12$ cm) by the higher frequency $n=3$ mode. In Fig. 5, the cross-power spectra between the reference diode at $z=-10.1$ cm and a diode at $z=0$ cm and a Mirnov probe, and also the auto-power spectrum of the reference diode, are shown. In Fig. 6, the absolute and normalized power spectra and phase profiles of two fundamental modes (F1 and F2) and their nonlinear coupling products (M-, M+, and Mh), are given. Finally, in Figs. 7 and 8, auto-bispectrum plots corresponding to Fig. 5 are shown.

The primary modes are: a strong central $m=1/n=1$ mode with much weaker $m=2,3/n=1$ components (f_1) and a strong $m=5/n=3$ mode with a somewhat smaller $3/3$ component (f_2). It is interesting that the second primary mode (f_2) is not a more regularly observed $4/3$ but a $5/3$ mode. Both of these primary modes have higher harmonics, which again interact nonlinearly with the other primary mode and its harmonics. The primary mode (f_1) is strongly distorted, creating a strong second harmonic. Higher harmonics of the two independent modes can also nonlinearly mix, so that in general one can obtain very complicated spectra with many peaks at frequencies $kf_2 \pm lf_1$ and with toroidal and poloidal mode numbers $kn_2 \pm ln_1$ and $km_2 \pm lm_1$, where k and l are integers: $k, l = 0, 1, 2, \dots$. Because of all these nonlinear interactions between the two primary modes and their harmonics, many products of this nonlinear coupling are observed as peaks in the power spectrum (Fig. 5).

There is a particularly strong nonlinear wave coupling of different modes on the $q=1$ surface. At least three $m=1/n=1$ modes are observed, each with a different phase velocity ($f_1=15.5$ kHz, $f_2-2f_1=12$ kHz, and $3f_1-f_2=3.5$ kHz). Similarly, several $m=2/n=2$, $m=3/n=3$, and $m=4/n=4$ modes are also observed, again with different phase velocities. Moreover, the modes with the same m - and n -numbers do not show the same profile form: e.g., the peak of the $1/1$ mode of the f_2-2f_1 nonlinear product is shifted outward from the peak of the $1/1$ primary mode from $z=5$ to 9 cm (compare F1 in Fig. 6a to Mh in Fig. 6b). This shift is probably caused by the f_2 mode being located outside of the $q=1$ surface and, therefore, pulling the f_2-2f_1 peak out toward the $q=1$ surface.

The difference nonlinear product (f_2-f_1, k_2-k_1) and the sum nonlinear product (f_2+f_1, k_2+k_1) always show a different amplitude. The amplitude of the saturated sum nonlinear interaction product is always much smaller than the amplitude of the difference product. This might be an indication that the two three-wave coupling coefficients for the two sidebands might

not be equal.

Most of the nonlinear coupling can be traced to a nonlinear interaction of two primary modes and their harmonics on the *same magnetic surface*. However, there are a strong experimental indications that nonlinear wave coupling can occur between two modes residing on two neighboring magnetic surfaces. This results in nonlinear coupling products that can reside on *new magnetic surfaces*. One such case might be an f_2+f_1 mode with $m=6/n=4$, and residing on the $q=1.5$ surface. This mode is created by the nonlinear interaction of $m=1/n=1$ (f_1) and $m=5/n=3$ (f_2) modes, where the new m - and n -mode numbers are given by $m=m_2+m_1$ and $n=n_2+n_1$. This nonlinear interaction between two modes on two different but neighboring surfaces has been observed in other discharges. This is an important effect, because the perturbation on a new rational surface could cause additional deterioration of the energy and particle transport.

Thus far, the evidence for three-wave coupling has been based on the observation that various frequencies (or modes) obey the three-wave coupling selection rule $f_a + f_b = f_c$. This approach is somewhat indirect in that it does not provide evidence of the phase coherence between three waves that are nonlinearly coupled. Direct evidence of such phase coupling is provided by the discrete auto-bispectrum, [11] which is defined as

$$B(f_a, f_b) = E[X^*(f_a)X^*(f_b)X(f_c=f_a+f_b)],$$

where $X(f)$ denotes the discrete Fourier transform of a fluctuation signal $x(t)$, and E denotes an expectation operator. The bispectrum may be viewed as a triple correlation in frequency space, and thus is sensitive to correlation or phase coherence that may exist between $X(f_a)$, $X(f_b)$, and $X(f_c=f_a+f_b)$. Since three-wave nonlinear interactions introduce such a phase coherence, a non-zero bispectrum at (f_a, f_b) provides further quantitative evidence of three-wave coupling involving f_a , f_b , and $f_c=f_a+f_b$. Conversely, if f_a , f_b , and $f_c=f_a+f_b$ are statistically independent modes, their phases would be independent and random and, thus, when the statistical averaging corresponding to the expectation operator is carried out, random phase mixing will cause the bispectrum to be zero. This property of the bispectrum follows from the properties of the cumulants. [12] In many cases, a normalized version of the bispectrum, called the bicoherence, is used to detect phase coherence. However, for the S_x time series data described in the previous discussion, we found that the bispectrum itself gave a sharper indication of the frequencies involved in the three-wave coupling.

Next in Figs. 7 and 8, we show the results of bispectral analysis of the soft x-ray signal, the power spectrum of which is given by the S_x curve in Fig. 5. Because of the symmetry

properties of the bispectrum, it is necessary to only plot $B(f_a, f_b)$ in the triangular region in the upper right-hand quadrant of the (f_a, f_b) plane. Both the three-dimensional plot of Fig. 7 and the contour plot of Fig. 8 indicate that there are several (f_a, f_b) coordinates characterized by a significant value of the bispectrum, supporting three-wave interactions between f_a , f_b , and $f_c = f_a + f_b$. Note that in Fig. 8, we have indicated the values of the (f_a, f_b) coordinates, and in Table II we have tabulated the interactions $f_a + f_b = f_c (= f_a + f_b)$. Virtually all of the frequencies identified in the S_x curve of Fig. 5 appear in Table II. Note that, while interpreting Figs. 7 and 8 and Table II, the auto-bispectrum is unable to discriminate between sum- and difference-frequency interactions. For example, the auto-bispectrum cannot distinguish between the sum-frequency interaction $10+5=15$ kHz, and the difference-frequency interaction $15-5=10$ kHz and $15-10=5$ kHz. All such interactions would be represented by a single peak at $f_a=10$ and $f_b=5$ kHz. In summary, a comparison of the S_x curve in Fig. 5 and the bispectral information contained in the Figs. 7 and 8 and Table II provides important additional evidence that we are indeed observing true three-wave interactions.

Another example of nonlinear mode coupling, now between a growing $m=1/n=1$ sawtooth precursor and a continuous $4/3$ mode with a strong $3/3$ component, is shown in Figs. 9 to 12. In this case the strongest nonlinear interaction, resulting in many nonlinear products, occurs immediately before the sawtooth crash, when, due to the reconnection process, the hot plasma region becomes very small, creating many strong harmonics of the $m=1/n=1$ sawtooth precursor. The cross-power spectrum and phase profiles of the two fundamentals and their harmonics immediately preceding the sawtooth crash are shown in Fig. 10 a and b. The $n=1$ mode is localized more strongly in the central part of the plasma (Fig. 10a) and the $n=3$ mode seems to be spread over the larger region of the minor radius (Fig. 10b). The spreading of the $n=3$ mode over the larger region means probably that the $m=4/n=3$ mode has a strong $m=5$ and 3 component. Note that the precursor harmonics are very strong, and that the number of peaks is increasing linearly with the m -number and is equal to $m+1$. For m =odd, there is a minimum in the center, and for m =even, a maximum. The phase difference across the plasma increases with the harmonic number, reflecting the increasing m -number, but the unexplained noise causes the evaluation of the phase for $z>0$ to become less certain.

At the time of the sawtooth crash we observe as many as four $m=1/n=1$ modes, each with a different frequency and phase velocity ($f_1=16.6$ kHz, $f_2-2f_1=11$ kHz, $4f_1-f_2=22.4$ kHz, and $2f_2-4f_1=21.6$ kHz). The profiles of these four $m=1/n=1$ modes is shown in Fig. 11b, with characteristic double peaks and a minimum in the center. Not explained is the fine splitting of the $m=1/n=1$ peaks into two peaks, observed most strongly in the $4f_1-f_2$ and $2f_2-$

$4f_1$ profiles. A possible cause for the fine splitting might be a non-monotonic q -profile with two or even three $q=1$ surfaces. The motional Stark effect (MSE) polarimetry measurement of the q -profile, shown in Fig. 11a, is not sensitive enough to be able to detect any multiplicity in the $q=1$ surfaces (the uncertainty in the central region being approximately $\Delta q=0.1$). At least three $2/2$ ($2f_1=33.2$ kHz, $f_2-f_1=27.4$ kHz, and $5f_1-f_2=39$ kHz), two $m=3/n=3$, and two $m=4/n=4$ modes are observed, each having a different frequency and phase velocity (Fig. 11c, top panel). Note that the profile complexity of the modes, e.g., the number of peaks, increases with the n -number, because the m -number also increases with n -number. The profile of the $n=2$ perturbations are dominated by the $m=2/n=2$ modes, and are therefore more central.

The $n=3$ perturbations display four peaks inside the $z=25$ cm surface, indicating a strong central $m=3/n=3$ component, with a strong additional peak for $z>25$ cm, representing $m=4/n=3$ fundamental (i_2). In the $n=4$ perturbations, five central peaks for $z<25$ cm are visible, indicating the presence of a strong $m=4/n=4$ component, and a weaker peak for $z>25$ cm, which represents a mode component outside the $q=1$ surface.

Note that at least eleven modes with $m=n=1, 2, 3, 4$ are observed at the $q=1$ surface, each of them of differing in frequency and therefore having a different phase velocity. The position of these modes agrees well with the position of the $q=1$ surface, localized in a similar discharge by the MSE measurement to be between $z=20$ and 25 cm (Fig. 11a). Similar mode multiplicity can be observed on other rational surfaces, but for $q=2$ and larger, it is more difficult to ascertain the m -number of the modes.

Finally, for the same sawtooth crash we show in Fig. 12 the time evolution of the auto power spectra of the peak of the profile for the $m=1/n=1$ sawtooth precursor (f_1), the independent mode $m=4/n=3$ (f_2), and for the two mixing products (f_2-f_1 and f_2+f_1). There we can see that the the amplitude of the mixing products increases roughly linearly with the precursor amplitude. This linearity appears to be lessened in the figure by the rather large contribution of the photon and other noise in the f_2-f_1 and f_2+f_1 signals. Subtracting that noise contribution (less than 100 nW) from the f_2-f_1 and f_2+f_1 amplitudes should improve the linearity of the relationship between f_1 and these two amplitudes. The sawtooth crash, probably through a slight change in the current profile, changes the saturation amplitude of the $m=4/n=3$ (f_2) mode.

The most prevalent case of the low- n nonlinear interactions is observed between the $n=1$ and $n=2$ modes. This simply follows from the fact that the probability of the mode growth seems to decrease with the n -number (Section 2.1). However, we did observe in similar high beta poloidal discharges mode mixing between the $n=2$ and $n=3$, $n=3$ and $n=4$, and $n=1$ and $n=3$ modes.

From these experimental data it is possible in general to find various parameters and coefficients of the three-wave coupling. Following Ritz et al. [5] the three-wave coupling can be described with two one-dimensional coupled wave equations, similar to the Hasegawa-Mima equation [13]:

$$\partial \Phi(k_{\pm}, t) / \partial t = (\gamma_{\pm} + i\omega_{\pm}) \Phi(k_{\pm}, t) + 1/2 \Lambda_{k_{\pm}}(k_1, k_2) \Phi(k_1, t) \Phi(k_2, t),$$

where $\Phi(k, t)$ is the spatial Fourier transform of the fluctuating field, $\phi(x, t)$, γ_{\pm} and $\omega_{\pm} = \omega_2 \pm \omega_1$ are the growth rates and the dispersion relations of two nonlinear interaction products, $k_{\pm} = k_2 \pm k_1$ are the two corresponding one-dimensional wave-numbers, and $\Lambda_{k_{\pm}}$ are two coupling coefficients for the three wave coupling. The subscript 1 and 2 refer to the two interacting fundamental modes.

From the measured fluctuation fields $\Phi(k_1, t)$, $\Phi(k_2, t)$, $\Phi(k_+, t)$, and $\Phi(k_-, t)$, and by manipulating the above coupled-wave equations by following the Ritz et al. prescription, [5] one could obtain the unknown γ 's, ω 's, and coupling coefficients Λ 's. In this case an attempt to find the unknown growth rates, dispersion relations, and coupling coefficients was not made for two reasons: there were not enough data (spatial points) and, what is more important, the method is a one-dimensional method and the experimental data presented here have at least two-dimensions (toroidal and poloidal). Moreover, the growth of the nonlinear products follows very closely the very slow growth of the sawtooth precursor, so that the data represent the slowly changing saturated states of all the waves involved.

In the future studies the work on the two-dimensional coupled wave equation, similar to Hasegawa-Mima equation, will be continued with the objective of finding the unknown γ 's, ω 's, and coupling coefficients Λ 's.

2.3. Fast Ion Losses During Weak Turbulence

An important question about the weak turbulence (three-wave coupling) is whether or not it contributes to any energy loss, and if so, through which channel. For that purpose, the neutron rate and the fast charge-exchange neutrals have been examined to find out if this turbulence causes fast ion loss. The data give a strong indication that the nonlinear mode interaction increases the energy losses. There is a clear time correlation between the onset and duration of the weak turbulence and a decrease in the slope of the neutron rate, increased ion losses in the neutral charge exchange efflux, and β saturation.

Unfortunately, because the nonlinear mode interaction occurs by definition simultaneously

with two primary modes, we cannot exclude them as the main cause of fast ion losses. However, if only one mode is present, the losses are considerably smaller in most cases. For example, a single strong mode after 520 ms and a short time earlier of a nonlinear three-wave coupling is shown in Fig. 13. Here, the three-wave coupling between 465 and 504 ms causes a large continuous drop in the neutron rate, whereas a stronger, saturated $n=1$ mode starting at 515 ms causes only a saturation in the neutron rate. The three-wave coupling occurs between a growing sawtooth ($m=1/n=1$) precursor, a saturated $n=2$ mode, and an $n=3$ mode. Normally, the neutron drop occurs only during the sawtooth crash and is absent during the growth of the $n=1$ sawtooth precursor. This sudden drop in the neutron rate due to the sawtooth crash is observed at 504 ms. The neutron rate decay between 465 and 504 ms, preceding the sawtooth crash, is obviously correlated and possibly caused by the three-wave interaction between the $n=1$, $n=2$, and $n=3$ modes, observed during this time. Neither the small ELM's at 464, 472, 479, and 490 ms, with an energy loss on the order of 1%, nor the giant ELM at 502 ms, with an energy loss on the order of 20%, cause any immediate loss in neutron rate.

A different case of three wave coupling is shown in Fig. 14. Four neutral beams are staggered from 250 to 400 ms. The β saturation starts around 440 to 450 ms, coincident with an onset of a stronger nonlinear interaction between two low- n modes. The increasing neutron rate saturates, and at the same time, a strong increase in the fast ion losses is observed in the charge-exchange signal, I_{cx} for energies 4 to 12 keV. The voltage applied to the electrostatic deflection plates of the charge-exchange analyzer was ramped linearly in time every 50 ms, corresponding to a range covering 0 to 60 keV in detected particle energy. [14] The triangular pattern of the voltage (and energy) sweep is shown over the data between 320 and 480 ms, with the 40 keV and zero energy points occurring at 433 ms and 458 ms respectively. From this figure it is clear that low to medium energy ions, from several keV to 15 keV, are preferentially lost during the weak turbulence (large bursts between 450 and 455 ms and between 460 and 465 ms).

The effect of the weak turbulence on the spectrum of the charge-exchange neutrals is shown in Fig. 15. The upper figure shows the spectrum of the charge-exchange flux before the onset of β -saturation, i.e., with no nonlinear interaction between two modes. The lower figure shows the spectrum during the weak turbulence. In the lower figure, the spectrum before the onset of weak turbulence (below 15 keV) is superimposed as a dashed line on the spectrum after the onset. The clear enhancement of the charge-exchange flux at energies less than 15 keV suggests that the weak turbulence does cause a loss of medium energy ions.

3. DISCUSSION

The nonlinear mode mixing has been mostly, but not exclusively, observed in the early and late β -saturation periods and in the β -collapse phase, where strong saturated and continuous modes typically develop. Though mostly observed in high- β discharges, the three-wave coupling is not a high- β effect; it has also been observed at low β 's, although much more rarely. The high- β parameters seem to facilitate more readily the destabilization of two different modes on two magnetic surfaces, and this is the main reason why these nonlinear interactions have been observed mostly in the high- β plasmas. At low- β the low- n modes are current driven, but as the β increases, the stability of the low- n modes also becomes increasingly dependent on the pressure gradients. In addition, the nonlinear interaction has been observed in PBX-M for various plasma shapes, implying that shaping alone cannot be responsible for the simultaneous destabilization of two independent modes and the recurrent observation of the three-wave coupling. This nonlinear interaction/weak turbulence is very often observed between two giant ELM's in high- β_{pol} discharges. It is not observed during the early β -rise phase, simply because during this phase the MHD activity is weak, and the condition for nonlinear interaction (the presence of two strong, saturated modes in the plasma) is not satisfied.

Because many different modes, some with the same m/n structure, can be localized during the three-wave coupling on the same rational magnetic surface, the question arises as to how all of these modes, having different toroidal and/or poloidal phase velocities, can coexist on the same rational surface. The modes of the same m/n structure but of different phase velocities, fixed by the selection rules or by toroidal coupling, are topologically mutually exclusive if they are tearing modes, because the islands cannot penetrate and flow through each other without break up of the magnetic surfaces constituting the islands. The mutual penetration of two islands would involve the break up and reconnection of magnetic field lines on a very short time scale, on the order of the mode oscillation period. The experimental data also show that the mode originating on a given magnetic surface q_k , having a component through toroidal coupling on another surface q_l , has a phase velocity inconsistent with the toroidal and/or poloidal rotation of the plasma and the phase velocity of the other mode originating on the surface q_l . These two modes on the surface q_l , because of their non-matching toroidal and/or poloidal phase velocities, would be again topologically mutually exclusive if they were both tearing modes. Matching of the phase velocities means that the modes are stationary in the plasma frame. For this reason, one can postulate that almost all the modes observed during the nonlinear wave interaction have a kink character, and that not many more than the two original modes, each residing on its own rational surface q_k or q_l , can themselves be tearing modes.

There is also the question of the localization of the nonlinear interaction. It has been shown in this paper that most of the nonlinear interactions occur with all three interacting modes residing on the same magnetic surface, or in the same narrow region of the plasma. However, some of the measurements described seem to indicate that the nonlinear interaction can also possibly occur between two modes residing on two neighboring magnetic surfaces, where the localization of the nonlinear interaction product is determined by the selection rule on the wave-number. This kind of nonlinear interaction has an important consequence in causing additional energy and particle loss, because the interaction product resides on a new surface different from the two surfaces of the original modes, and thereby enlarges the volume where losses can occur. Furthermore, this means that through the toroidally induced modes, these perturbations and their nonlinear interaction products can spread over a substantial part of the plasma volume. Here again the selection rule on the phase velocity (or frequency) has to be satisfied, and since this phase velocity does not in general match the local toroidal and/or poloidal plasma velocity, one can surmise once more that this nonlinear product should have the kink character.

The experimental results and their phenomenological interpretations lead us now to the following picture. The two primary modes are most probably the tearing modes, residing on two different magnetic surfaces. Their phase velocities appear to be matched to the local plasma velocities (combination of poloidal and toroidal rotation), which have different values on the two magnetic surfaces. Through toroidal coupling, the two primary modes induce secondary modes on other magnetic surfaces. It is not clear if the toroidally induced modes are tearing or kink modes, because their phase velocities are determined by the toroidal coupling and the phase velocities of the primary modes, and they do not need to match the local plasma velocities. The modes created by the nonlinear interaction between these two primary modes and their toroidally induced modes should all have a kink character, because their phase velocities do not in general match neither the phase velocities of the primary and the toroidally induced modes, nor the local plasma velocities. The main reason for this mismatch is the inhomogeneous distribution of the local plasma velocity across the minor radius.

It has been shown in the paper that during the three-wave coupling, one can observe a decrease in the neutron rate and an enhanced loss of medium energy ions. No comparable observation could be made on the electron losses, although one can assume that the electrons would also show enhanced losses during the three-wave coupling. The physical mechanism for the enhanced losses has not been identified, especially if the non-linear products of the three-wave coupling are kink modes. Nothing on the possibility of enhanced stochasticity or ergodization of the magnetic surfaces is known. Recently, Hegna and Callen proposed a mechanism for the loss enhancement, postulating increased stochasticity around the separatrices

of the magnetic islands driven by bootstrap currents. [15, 16] The applicability of this theory to the presented results of the three-wave coupling is questionable, however, because the theory is based solely on tearing modes and excludes kink modes.

Acknowledgments:

This work was supported by the U S Department of Energy Contract No. DE-AC02-76-CHO-3073.

- (a) Grumman Aerospace Corporation, Bethpage, NY, USA
- (b) ARACOR, Sunnyvale, CA
- (c) Fusion Physics & Technology, Torrance, CA, USA

REFERENCES

- [1] BELL, R.E., ASAKURA, N., BERNABEI, S., et al., *Phys. Fluids B* **2**, 1271 (1990).
- [2] SAUTHOFF, S., ASAKURA, N., BELL, R., et al., *Proceedings of the 13th Intern. Conf., on Plasma Phys. and Contr. Nucl. Fus. Research*, (Washington, DC, October 1990), (IAEA, Vienna, Austria) Vol. I, 709 (1991).
- [3] SESNIC, S., KAYE, S., AND OKABAYASHI, M., *Proceedings of the 18th European Conference on Controlled Fusion and Plasma Physics*, Berlin, 3-7 June, 1991; *Europhysics Conference Abstracts*, V. 15, Part II, p. II-97.
- [4] ASSADI, S., PRAGER, S.C., and SIDIKAM, K.L., *Phys. Rev. Lett.*, **69**, 281 (1992).
- [5] RITZ, CH. P., POWERS, E.J., and BENGSTON, R.D., *Phys. Fluids B* **1**, 153 (1989).
- [6] SESNIC, S., HOLLAND, A., KAITA, R., et al., *Nucl. Fusion*, to be published
- [7] HEIDBRINK, W.W., *Rev. Sci. Instrum.* **57**, 1769 (1986).
- [8] KUGEL, H.W., GAMMEL, G.M., KAITA, R., REUSCH, M.F., and ROBERTS, D.W., *Rev. Sci. Instrum.*, **59**, 1635 (1988).
- [9] LEVINTON, F., FONCK, R., GAMMEL, G.M., et al., *Phys. Rev. Lett.*, **63** 2060 (1989).
- [10] SESNIC, S., HOLLAND, A., KAYE, S., DUPERREX, P.-A., GAMMEL, G., and OKABAYASHI, M., *Bull. Am. Phys. Soc.* **34**, 2048 (1989).
- [11] KIM, Y.C. and POWERS, E.J., *Phys. Fluids*, **21**, 1452 (1978).
- [12] KIM, Y.C. and POWERS, E.J., *IEEE Trans. Plasma Sci.*, **PS-7**, 120 (1979).
- [13] HASEGAWA and MIMA, K., *Phys. Rev. Lett.* **39**, 205 (1977).

- [14] KAITA, R., GOLDSTON, R.J., MEYERHOFER, D., and ERIDON, J., *Rev. Sci. Instrum.* **52**, 1795 (1981).
- [15] HEGNA, C.C. and CALLEN, J.D., *Phys. Fluids B* **4**, 1855 (1992).
- [16] ZUOYANG CHANG, FREDRICKSON, E.D., CALLEN, J.D., et al., *Proceedings of the 20th European Conference on Controlled Fusion and Plasma Physics, Lisboa, 26-30 July, 1993; European Conference Abstracts, V. 17C, Part I, p. I-207 (1993).*

FIGURE CAPTIONS:

Fig. 1. Equilibrium magnetic surfaces for a high β_{pol} discharge with the low-n mode weak turbulence. The lines-of sight of individual soft x-ray diodes, used in MHD analysis, are also shown. Position of a given diode, z , is defined as the vertical hight from the midplane to the intersection between the diode line-of-sight and a vertical line at $R=165$ cm.

Fig. 2. Power spectrum, S_x , normalized power spectrum, S_x/S_0 , and phase, ϕ , profiles for a weak $n=1$ (a) and large (b) mode. Φ describes the calculated equivalent photon noise profile. A considerable part of the indicated error bars in this and the following figures is not caused by the noise, but comes from the true time variation of the mode amplitude. Statistical error in phase in the central part for all figures is less than $\pm 5^\circ$.

Fig. 3. Power spectrum, S_x , normalized power spectrum, S_x/S_0 , and phase, ϕ , profiles for a large $n=2$ (a) and $n=3$ (b) modes.

Fig. 4. Magnetic probe signal, I_M , and soft x-ray signals, I_x , with vertical position of the diode, z , as a parameter during nonlinear mode coupling.

Fig. 5. Auto-power spectrum of one diode ($z=-10.1$ cm), S_x , and cross-power spectra of the same diode with another diode, C_{12} , and with magnetic probe, C_{xM} , obtained between 566 and 570 ms of Fig. 5.

Fig. 6. Power spectra, S_x , normalized power spectra, S_x/S_0 , and phase, ϕ , profiles for a two "fundamental" modes f_1 and f_2 and their three non-linear coupling products: f_2-f_1 (M-), f_2+f_1 (M+), and f_2-2f_1 (Mh). Mode f_1 has a strong $m=1/n=1$ component but f_3 has two strong components: $5/3$ and $3/3$.

Fig. 7. Three dimensional plot of the auto-bispectrum of the time series corresponding to the S_x power spectrum in Fig. 5.

Fig. 8. Contour plot of the auto-bispectrum of the time series corresponding to the S_x power spectrum in Fig. 5. Note that the (f_a, f_b) coordinates of the bispectrum peaks are indicated.

Fig. 9. Time evolution of cross-power spectrum contours, C_{xx} , of two soft x-ray signals during nonlinear coupling between continuous mode f_2 and sawtooth precursor f_1 . m-number in parenthesis means that the identification of m-number is weak. Where only n-number is given, the m-number identification was impossible.

Fig. 10. Soft x-ray power spectrum and phase profiles of (a) the sawtooth precursor (1) and its harmonics (2, 3, ..6) and (b) of the other fundamental (1) and its harmonic (2). The profiles are evaluated at $t=534$ ms (see Fig. 7) immediately before the sawtooth crash.

Fig. 11. Soft x-ray power spectrum and normalized power spectrum profiles of (b) four $n=1$ modes: sawtooth precursor (f_1) and three nonlinear coupled modes (f_2-2f_1 , $4f_1-f_2$, and $2f_2-4f_1$) and of (c) for $n=2, 3$, and 4 modes: fundamental (f_2), harmonics ($2f_1$, $3f_1$, $4f_1$), and nonlinear coupled modes (f_2-f_1 , f_2+f_1 , and $5f_1-f_2$). The profiles are evaluated at $t=534$ ms (Fig. 8) immediately before the sawtooth crash. The profile of the safety parameter, $q(z)$, measured in a similar discharge using MSE diagnostic is also shown (a). The flux surfaces corresponding to the measured q -profile are shown in Fig. 1.

Fig. 12. Time evolution of power spectrum amplitude of the fundamental modes, f_1 and f_2 , and two nonlinearly coupled modes, f_2-f_1 and f_2+f_1 , during the sawtooth precursor growth of Fig 7.

Fig. 13. The effect of a large, single $n=1$ mode ($t>515$ ms) and of nonlinear interaction between two low- n modes ($450<t<505$ ms) on the neutron rate. The large event at 504 ms is a sawtooth and the small drops in the second trace (at 464, 472, 479, 490, and 502 ms) represent small ELM's. The first trace, representing an off-center diode, is filtered with a 2 kHz high-pass filter.

Fig. 14. Early and late β saturation shown in average density, $\langle n_e \rangle$, SX intensity, I_x , Mirnov coil, I_M , neutron rate signals, I_n , and charge exchange flux, $I_{c.x.}$. Charge exchange detector energy is being swept as indicated by E_i signal. Strong neutron rate saturation between 440 to 480 ms coincides with weak turbulence and large fast ion losses. The short spikes on I_n signals are hard x-rays caused by runaways being ejected during the sawtooth crash.

Fig. 15. Comparison of charge-exchange efflux before (A) and or during (B) weak turbulence.

Table I

Parameters of Low-n Modes

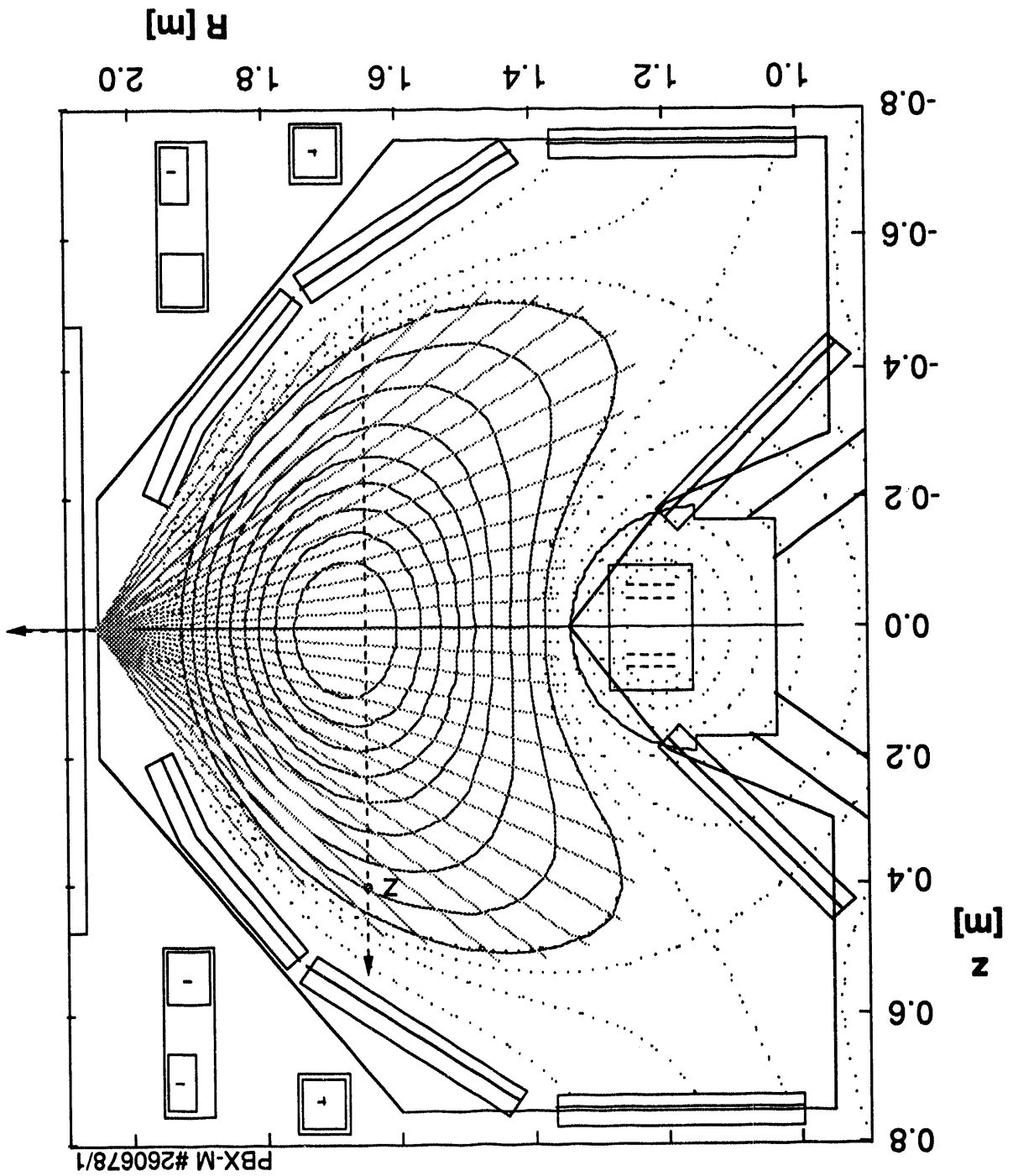
Mode at $q=1$, m/n	1/1	2/2	3/3	4/4
f [kHz]	7.3/15	27.5	44	55
z_{\max} (for $q>1$)	45	33	30	27
z_{\min} (for $q>1$)	55?	42	37	32
Mode at z_{\max} , m/n	2, 3?/1	3/2	4/3	5/4
Times occurred in 17 discharges	11	7	4	1

Table II

Tabulation of the various three-wave interactions $f_a + f_b = f_c (=f_a + f_b)$ corresponding to the peaks identified by the letters a, b, c, d, e,.....q in Fig. 9.

Index	f_a	f_b	$f_a + f_b$
a	f_2	f_2	$2f_2$
b	f_2	$2f_1$	$f_2 + 2f_1$
c	f_2	$f_2 - f_1$	$2f_2 - f_1$
d	f_2	f_1	$f_1 + f_2$
e	f_2	$f_2 - 2f_1$	$2f_2 - 2f_1$
f	f_2	$3f_1 - f_2$	$3f_1$
g	$2f_2 - 3f_1$	$3f_1 - f_2$	f_2
h	$2f_1$	$2f_1$	$4f_1$
i	$2f_1$	$f_2 - f_1$	$f_2 + f_1$
j	$2f_1$	f_1	$3f_1$
k	$2f_1$	$f_2 - 2f_1$	f_2
l	$f_2 - f_1$	f_1	f_2
m	f_1	f_1	$2f_1$
n	f_1	$f_2 - 2f_1$	$f_2 - f_1$
o	f_1	$3f_1 - f_2$	$4f_1 - f_2$
p	$f_2 - 2f_1$	$3f_1 - f_2$	f_1
q	$3f_1 - f_2$	$3f_1 - f_2$	$6f_1 - 2f_2$

Fig. 1



PBX-M #260678/1

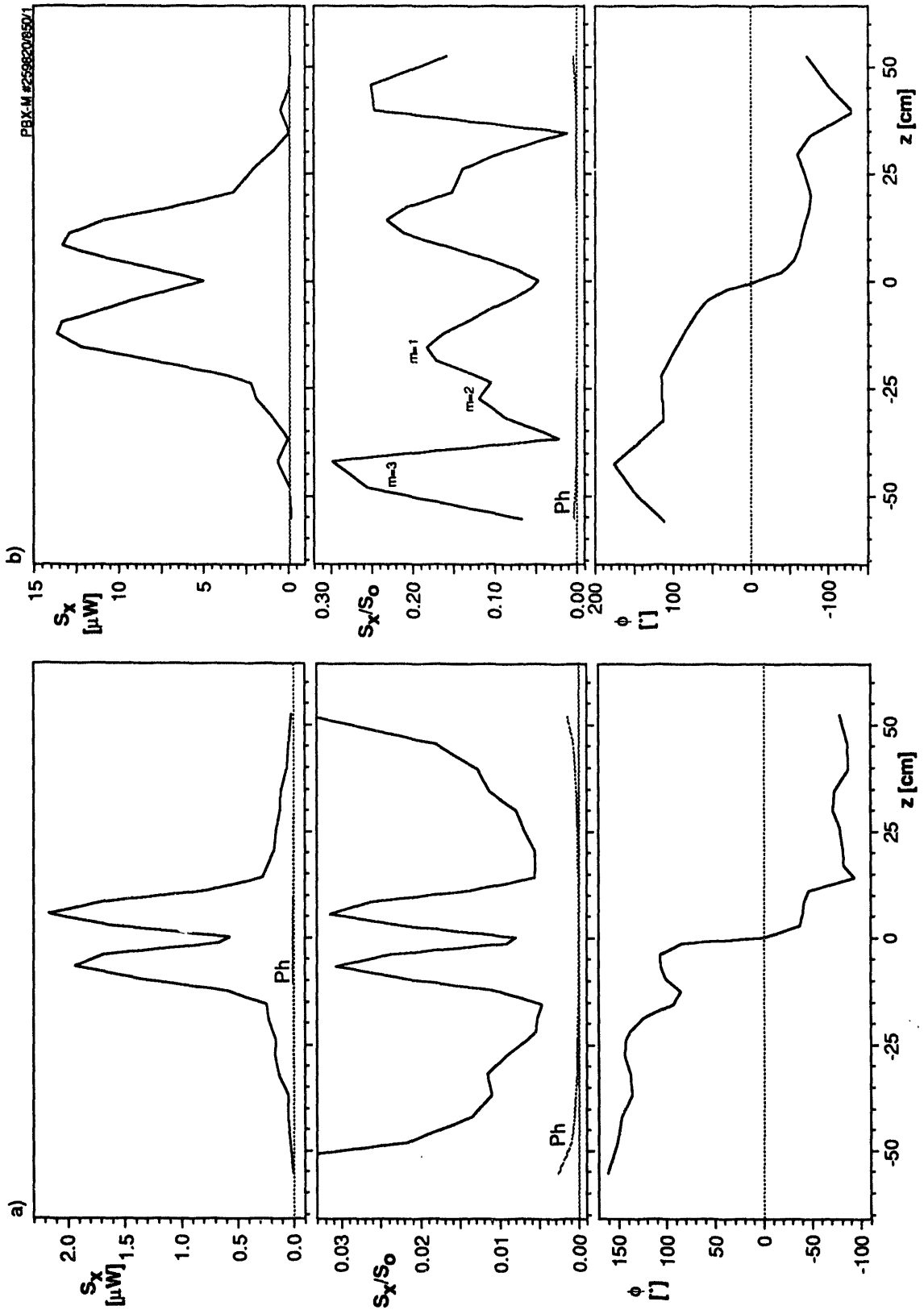


Fig. 2

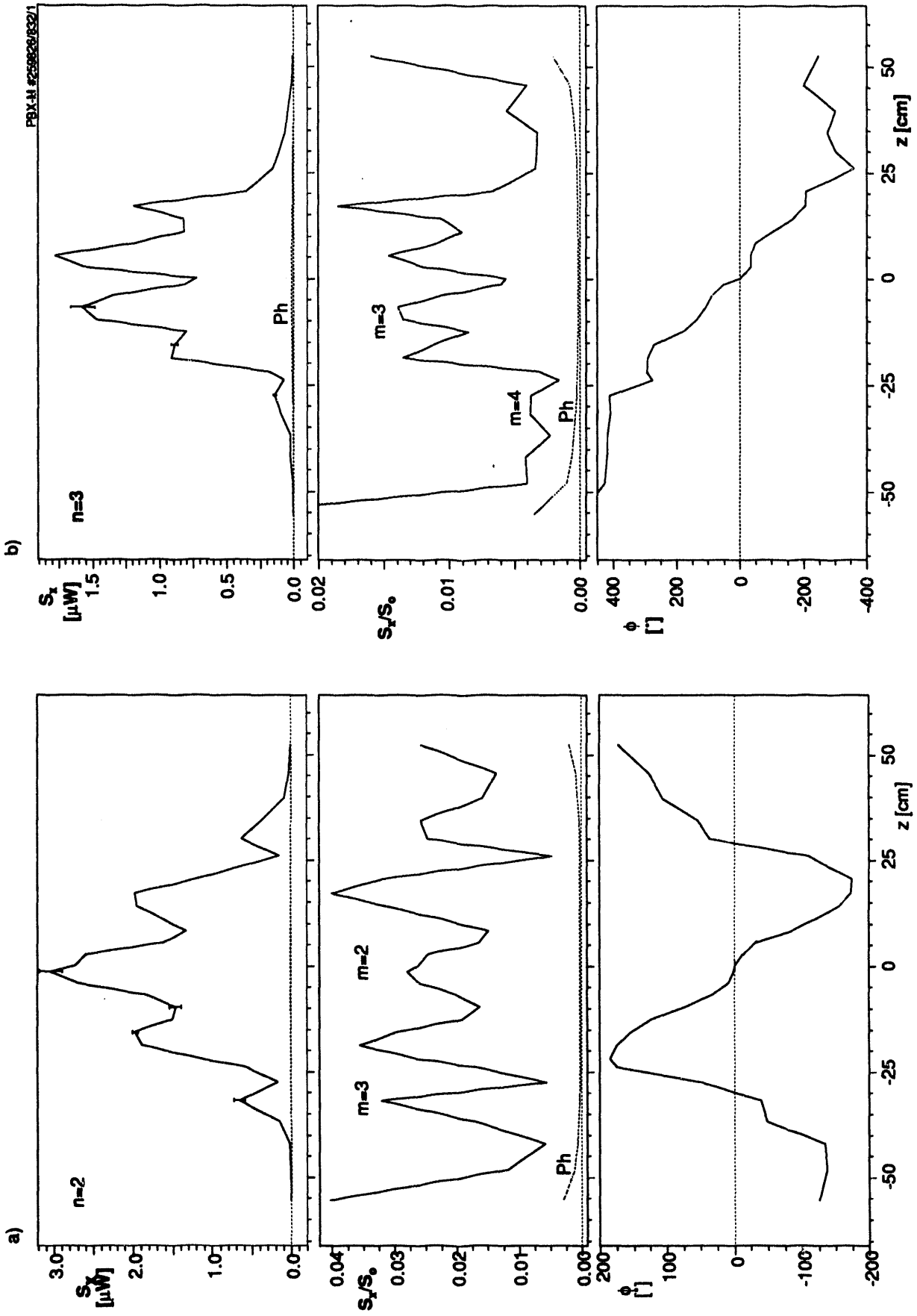


Fig. 3

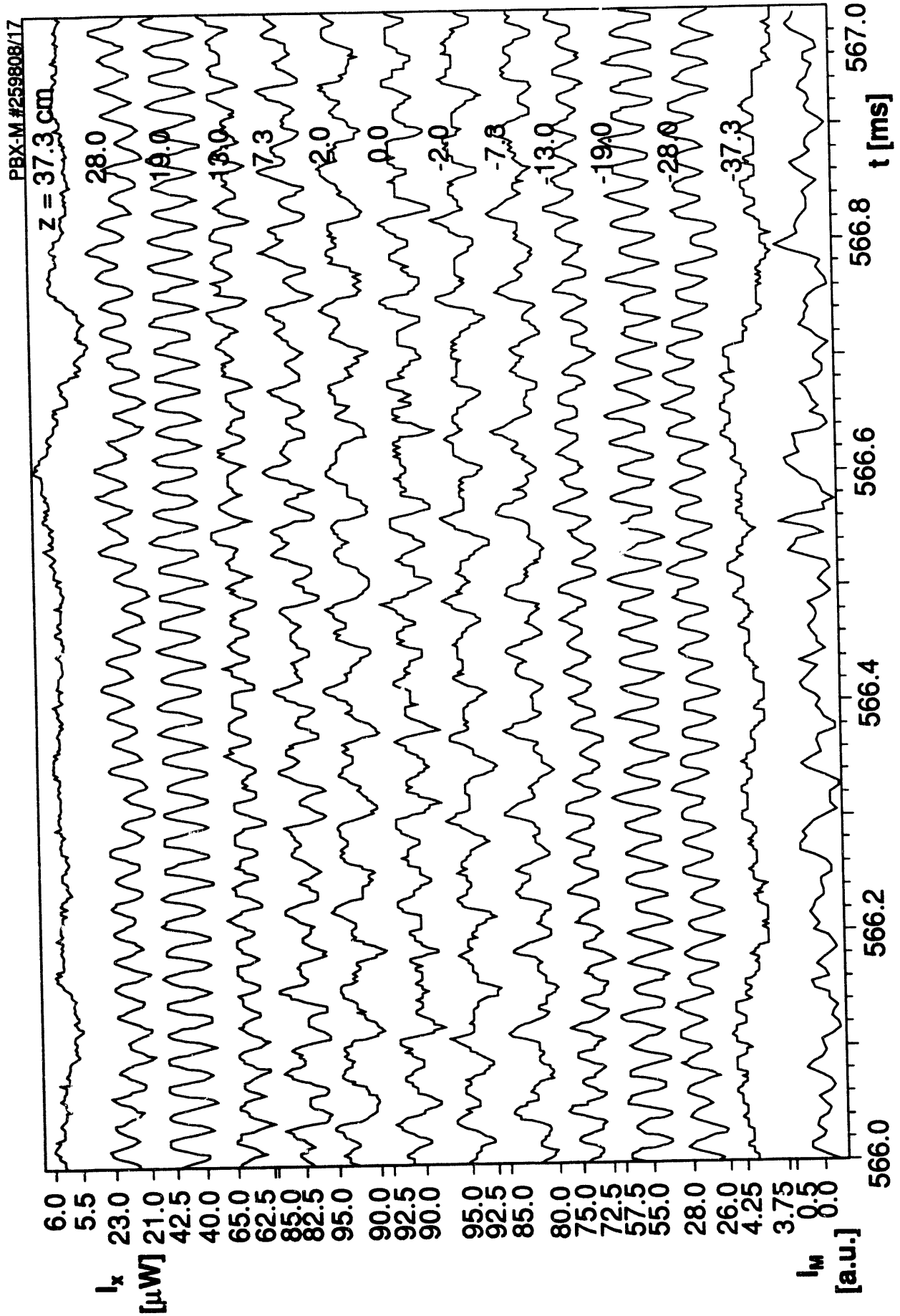


Fig. 4

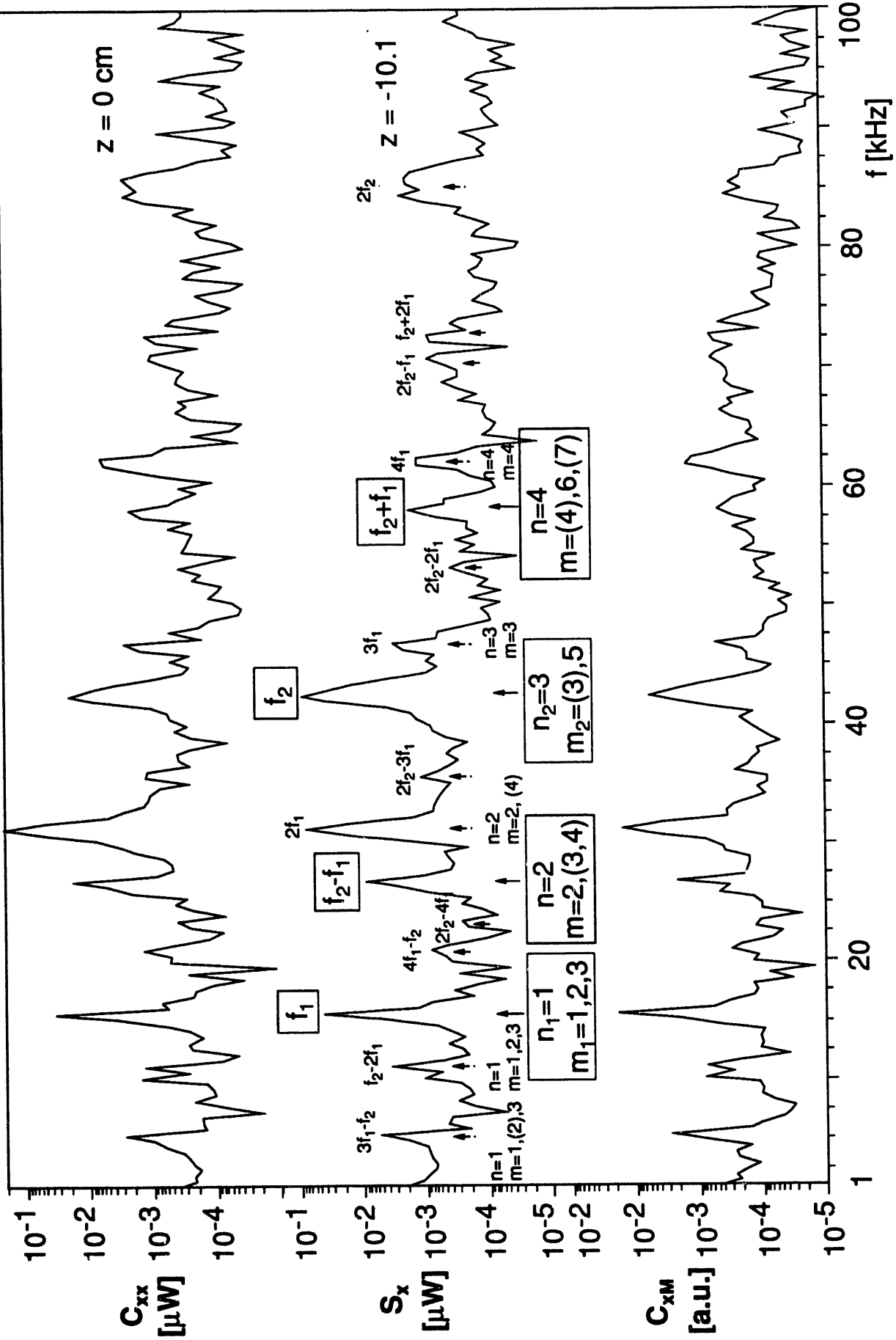


Fig. 5

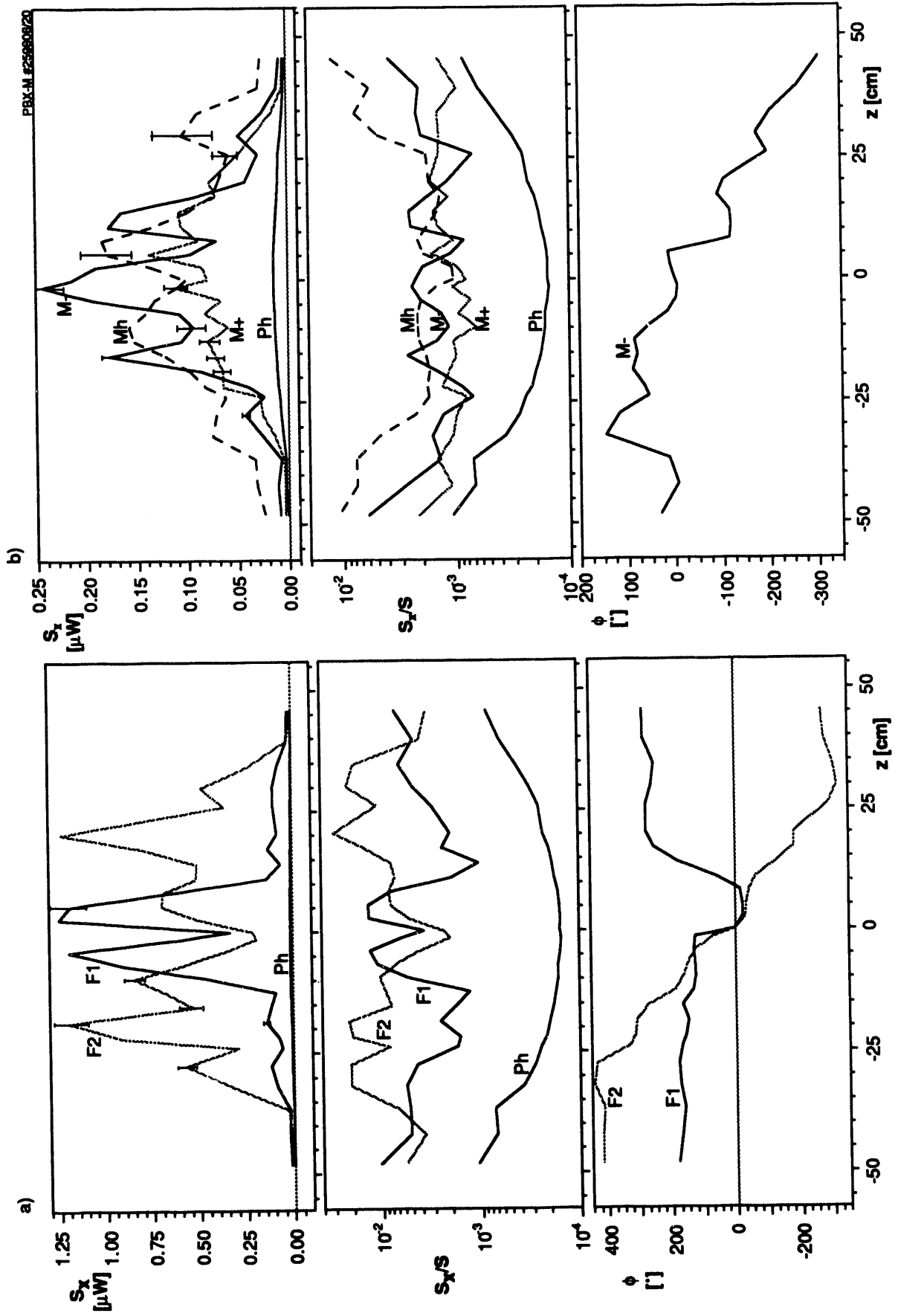


Fig. 6

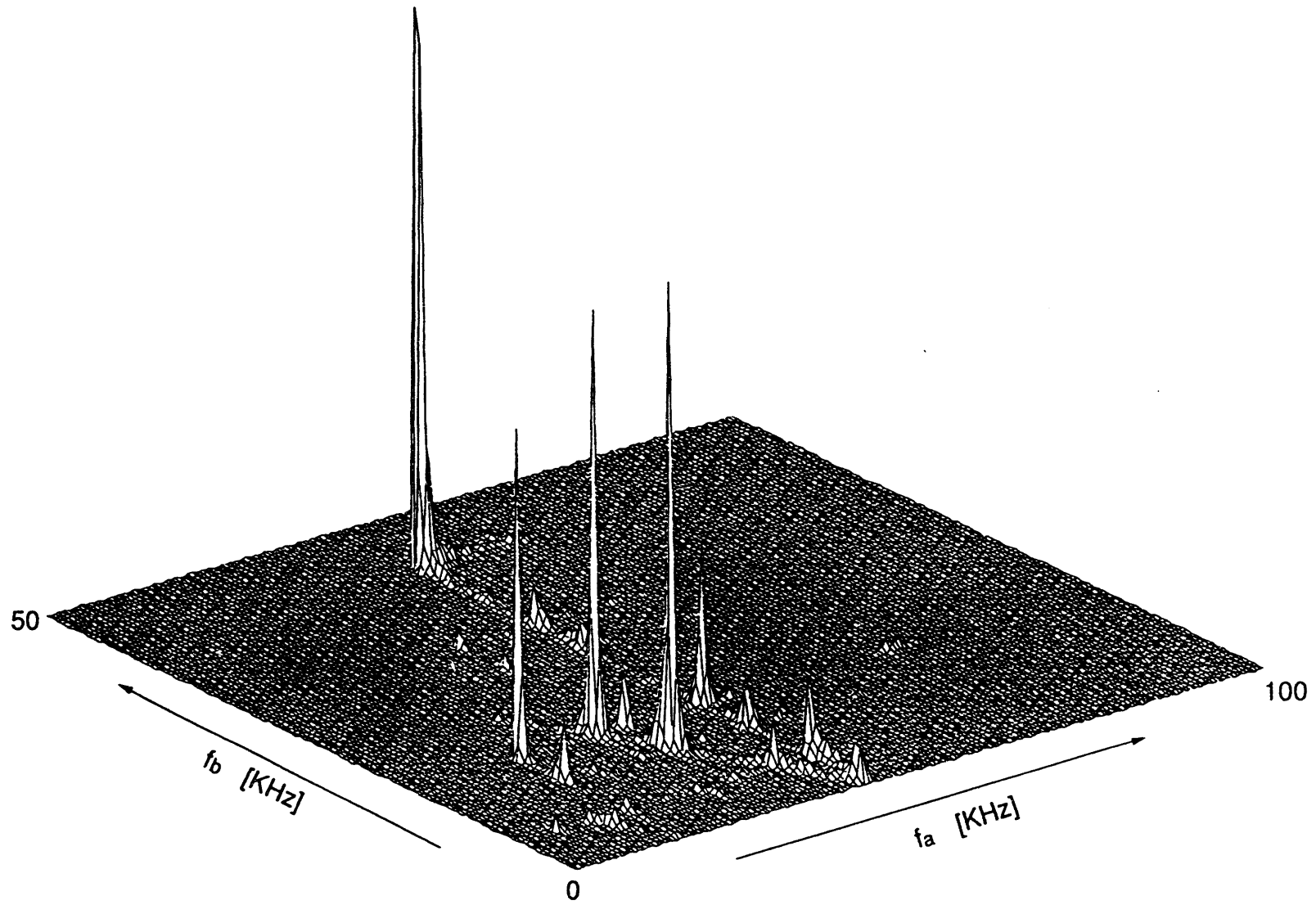


Fig. 7

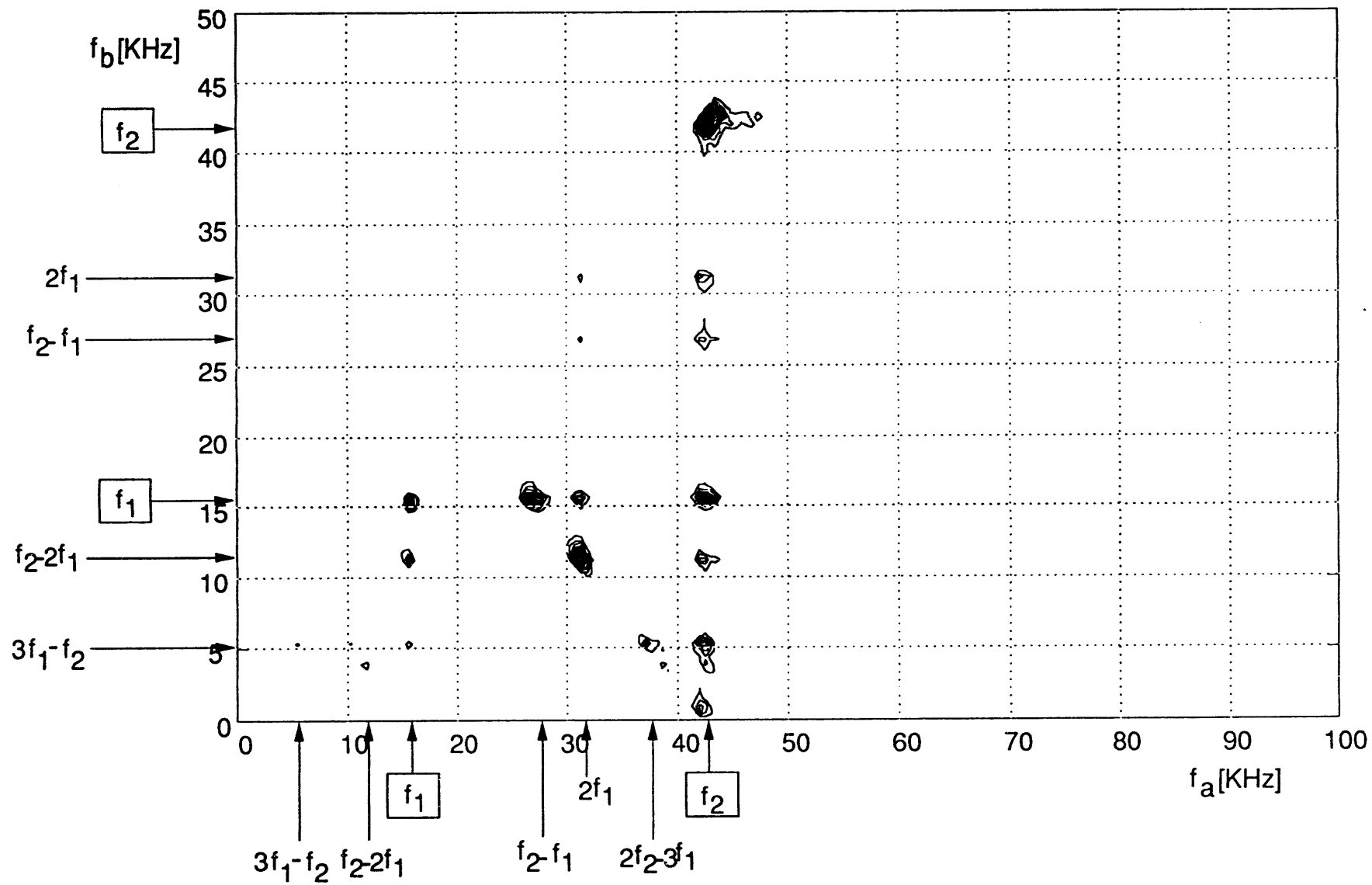


Fig. 8

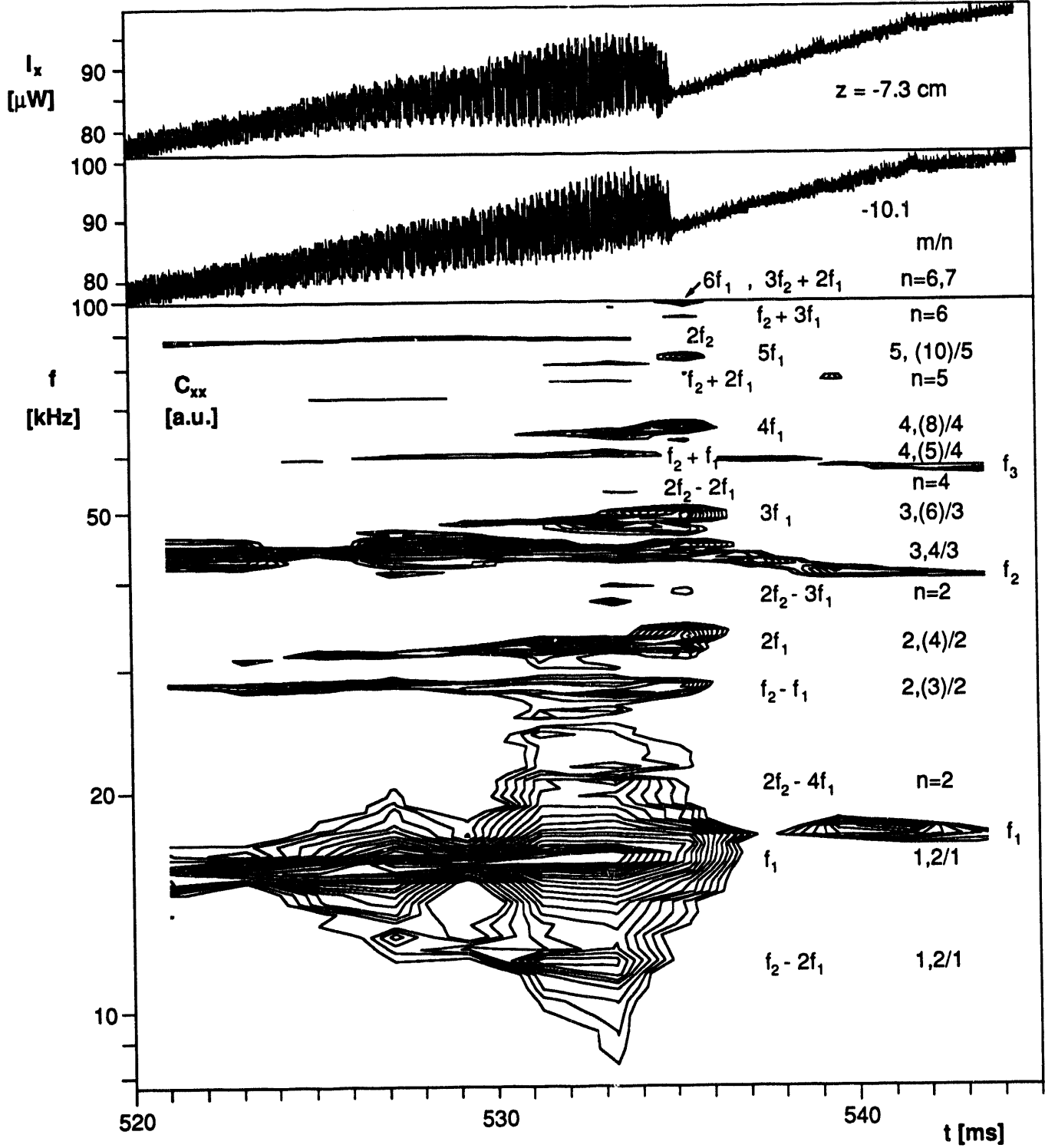


Fig. 9

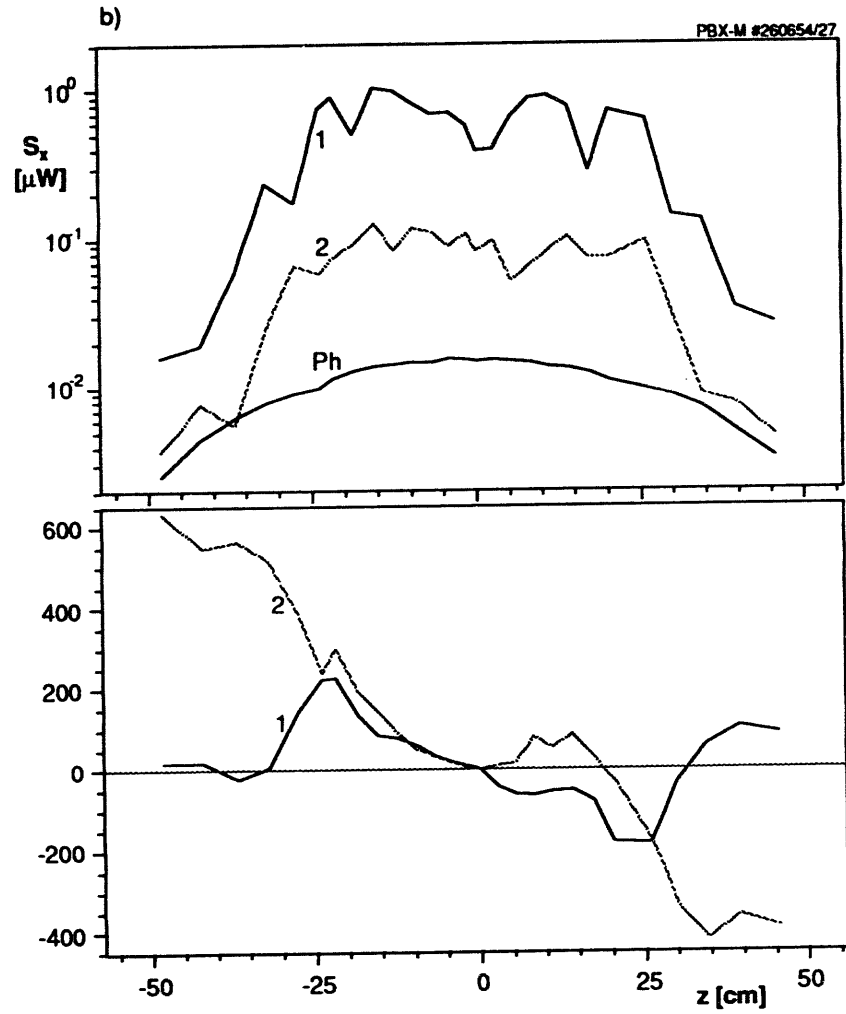
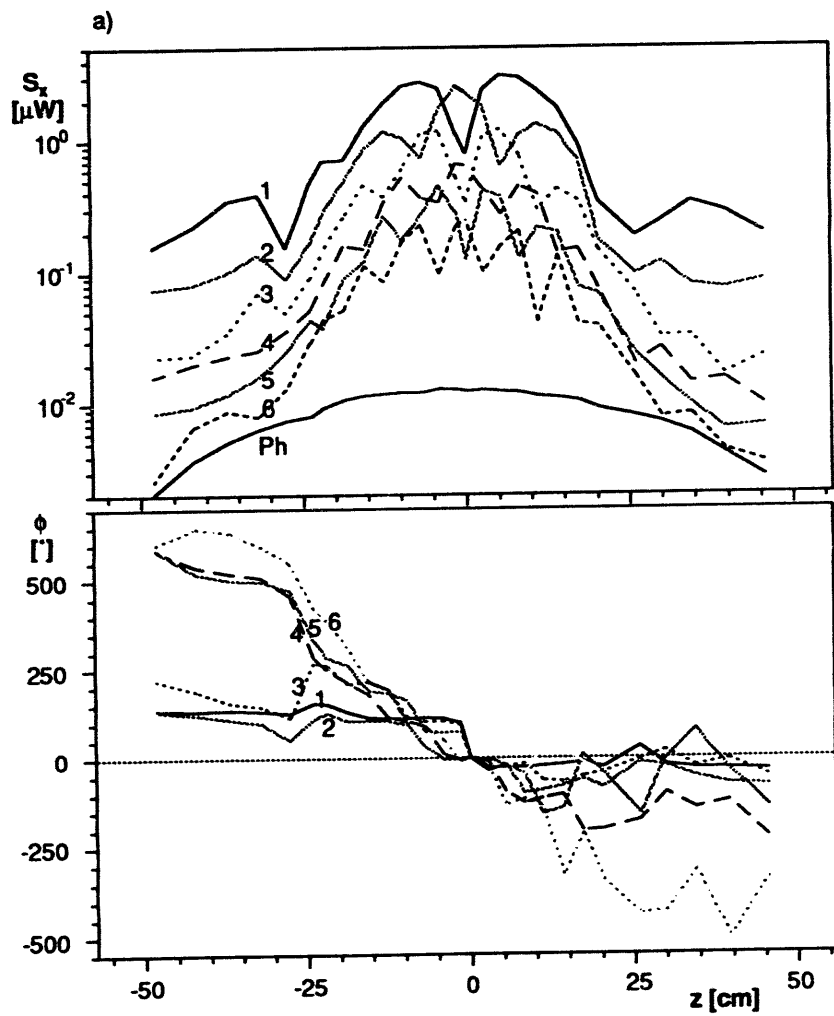


Fig. 10

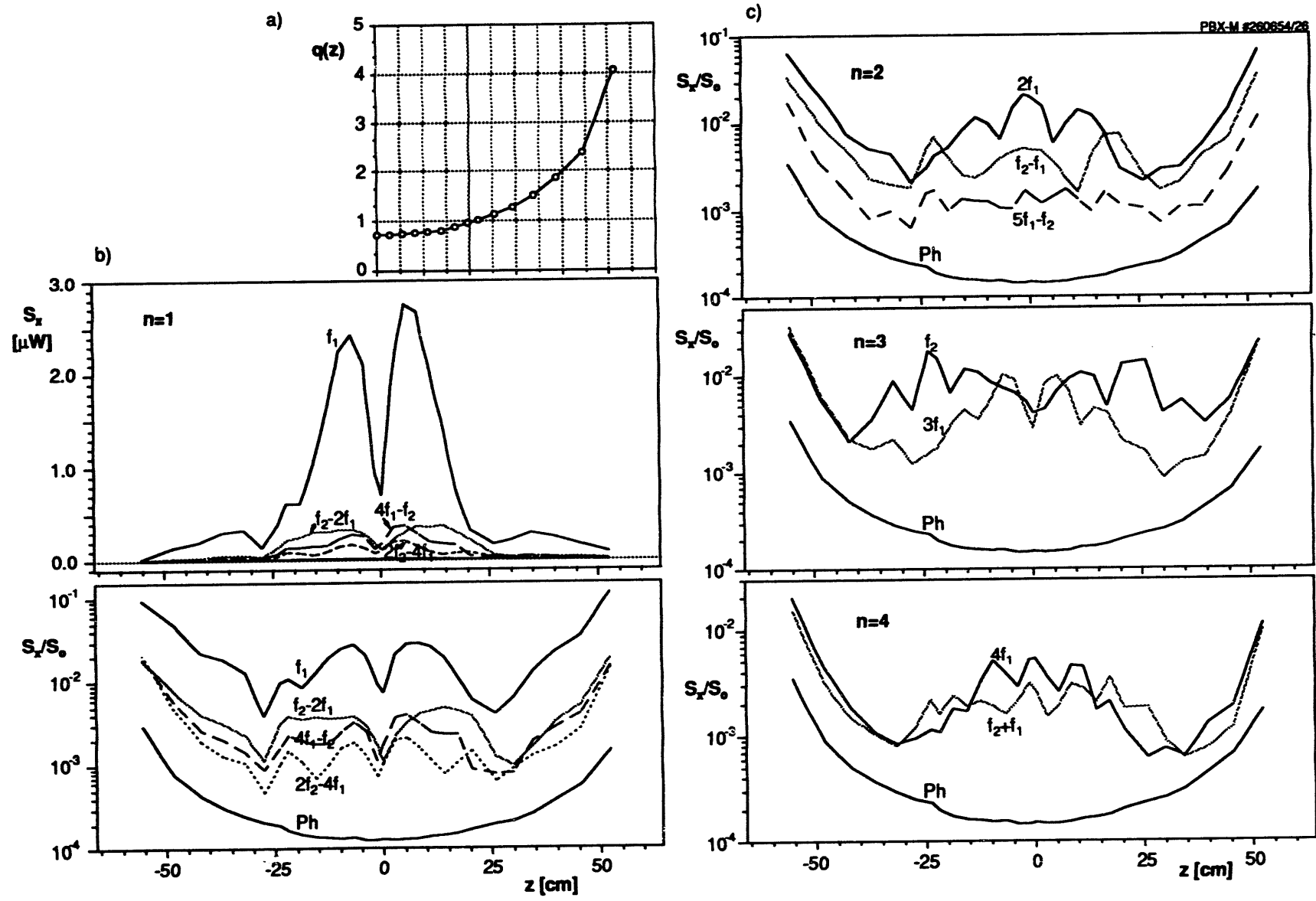


Fig. 11

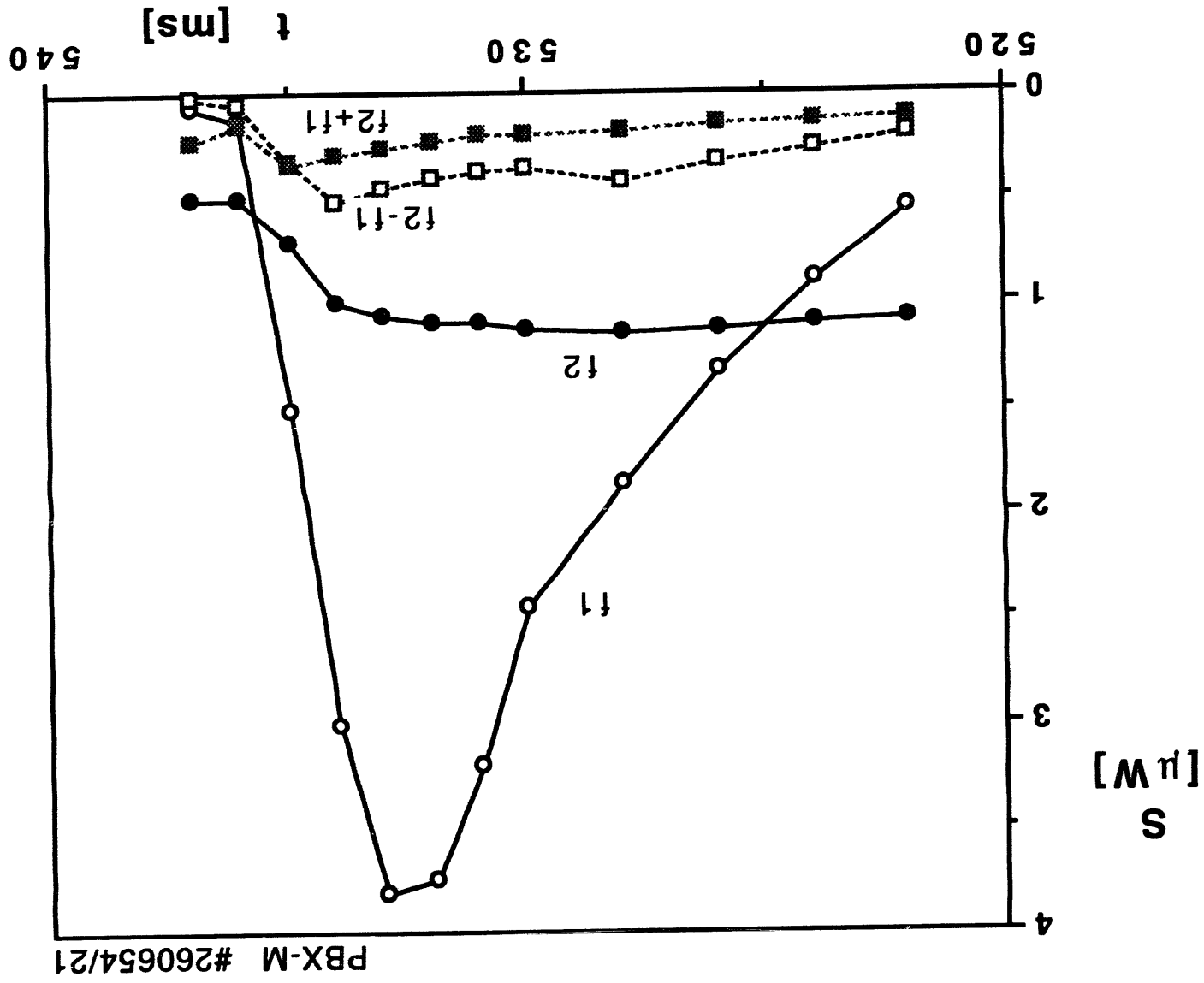


Fig. 12

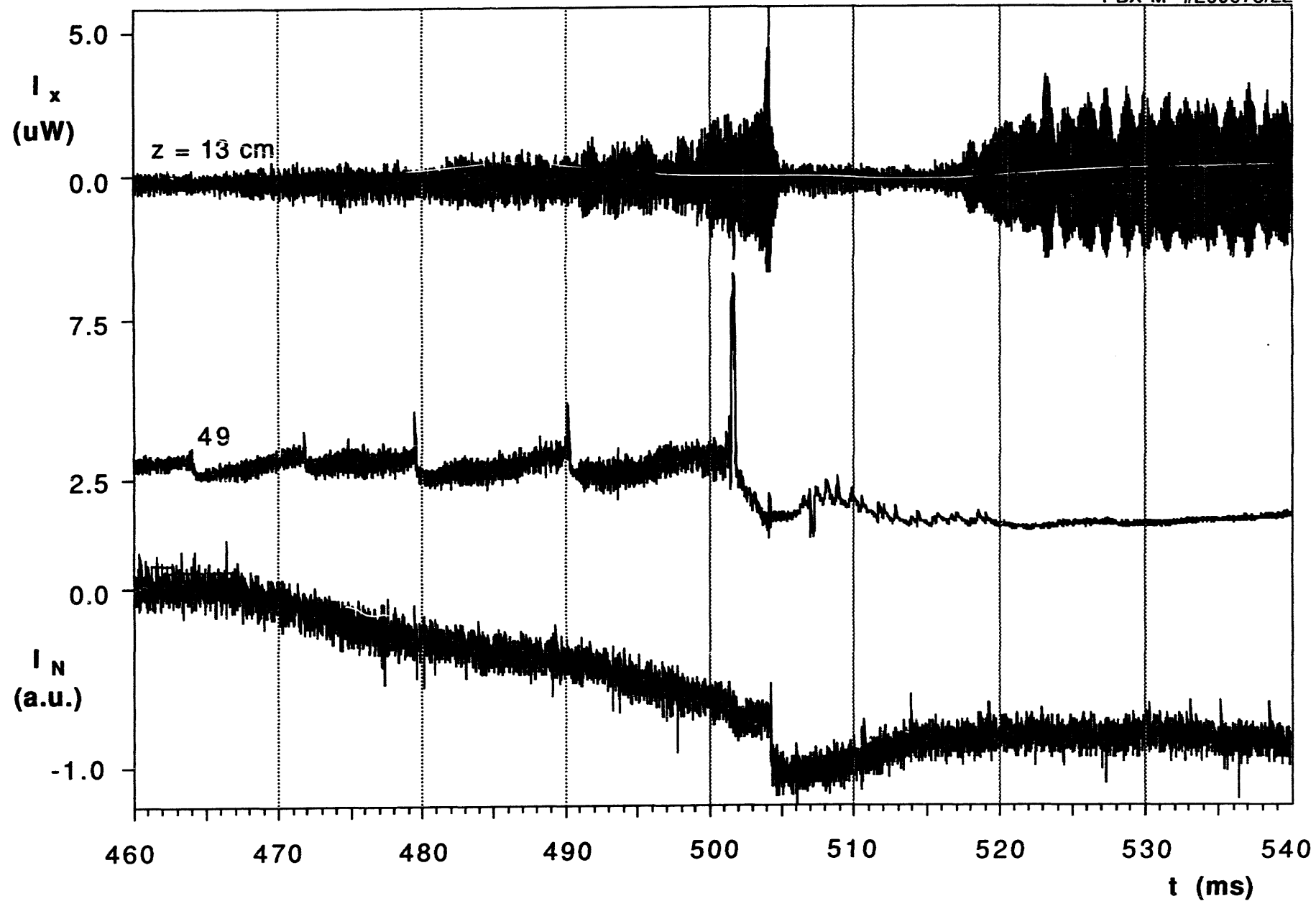


Fig. 13

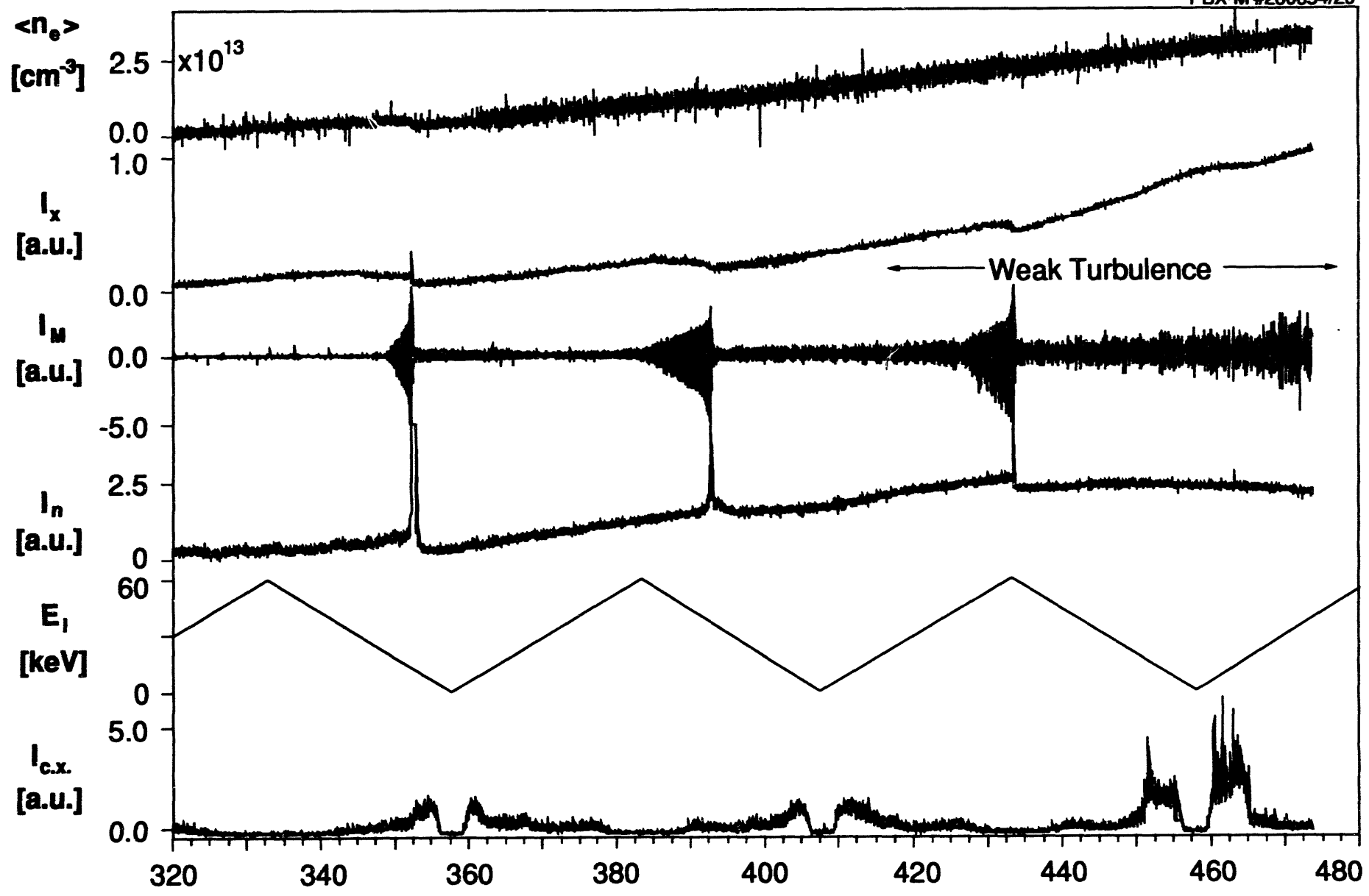


Fig. 14

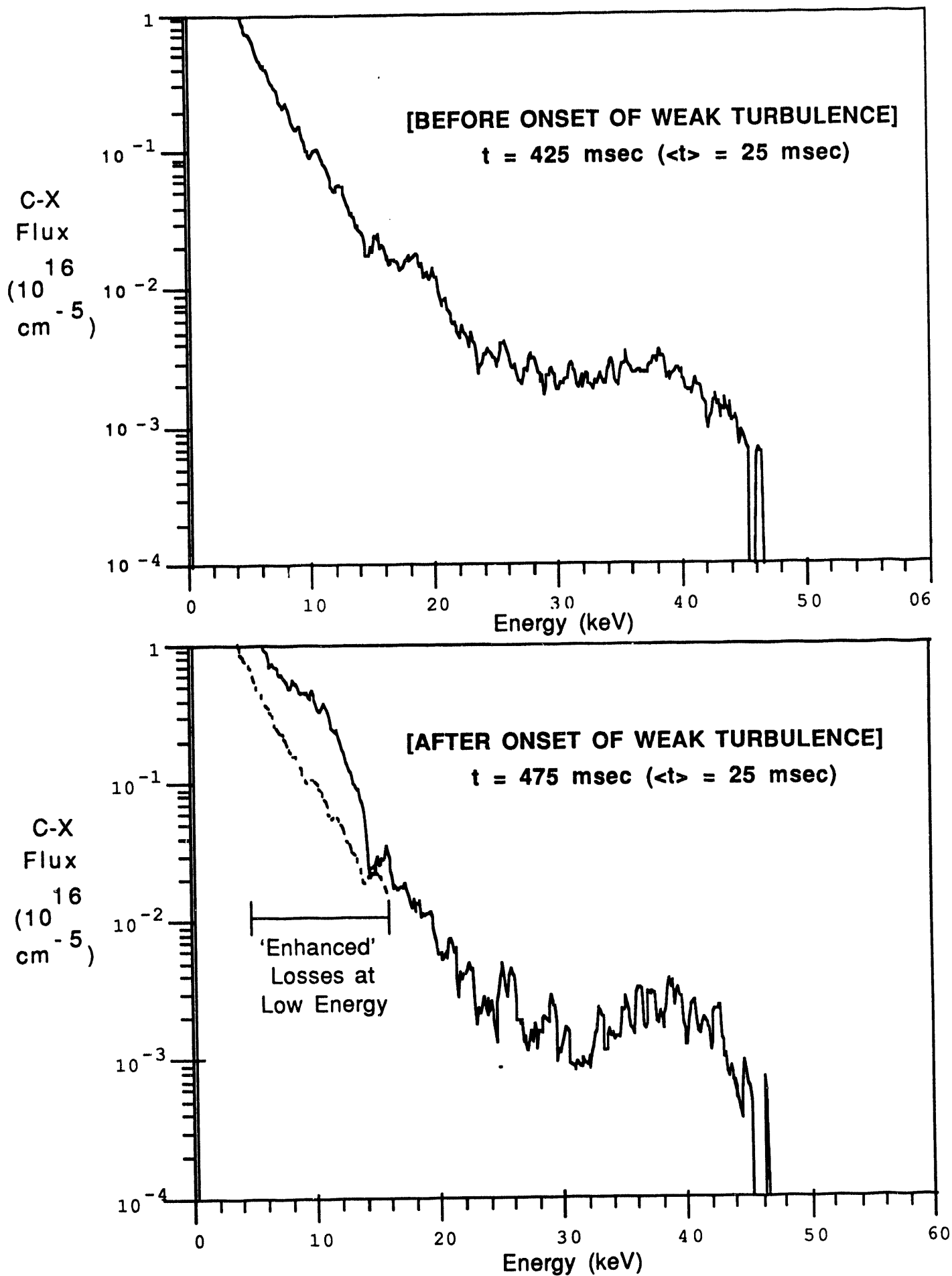


Fig. 15

EXTERNAL DISTRIBUTION IN ADDITION TO UC-420

Dr. F. Paoloni, Univ. of Wollongong, AUSTRALIA
 Prof. M.H. Brennan, Univ. of Sydney, AUSTRALIA
 Plasma Research Lab., Australian Nat. Univ., AUSTRALIA
 Prof. I.R. Jones, Flinders Univ, AUSTRALIA
 Prof. F. Cap, Inst. for Theoretical Physics, AUSTRIA
 Prof. M. Heindler, Institut für Theoretische Physik, AUSTRIA
 Prof. M. Goossens, Astronomisch Instituut, BELGIUM
 Ecole Royale Militaire, Lab. de Phy. Plasmas, BELGIUM
 Commission-European, DG. XII-Fusion Prog., BELGIUM
 Prof. R. Bouciqué, Rijksuniversiteit Gent, BELGIUM
 Dr. P.H. Sakanaka, Instituto Fisica, BRAZIL
 Prof. Dr. I.C. Nascimento, Instituto Fisica, Sao Paulo, BRAZIL
 Instituto Nacional De Pesquisas Espaciais-INPE, BRAZIL
 Documents Office, Atomic Energy of Canada Ltd., CANADA
 Ms. M. Morin, CCFM/Tokamak de Varennes, CANADA
 Dr. M.P. Bachynski, MPB Technologies, Inc., CANADA
 Dr. H.M. Skarsgard, Univ. of Saskatchewan, CANADA
 Prof. J. Teichmann, Univ. of Montreal, CANADA
 Prof. S.R. Sreenivasan, Univ. of Calgary, CANADA
 Prof. T.W. Johnston, INRS-Energie, CANADA
 Dr. R. Bolton, Centre canadien de fusion magnétique, CANADA
 Dr. C.R. James,, Univ. of Alberta, CANADA
 Dr. P. Lukác, Komenského Univerzita, CZECHO-SLOVAKIA
 The Librarian, Culham Laboratory, ENGLAND
 Library, R61, Rutherford Appleton Laboratory, ENGLAND
 Mrs. S.A. Hutchinson, JET Library, ENGLAND
 Dr. S.C. Sharma, Univ. of South Pacific, FIJI ISLANDS
 P. Mähönen, Univ. of Helsinki, FINLAND
 Prof. M.N. Bussac, Ecole Polytechnique,, FRANCE
 C. Mouttet, Lab. de Physique des Milieux Ionisés, FRANCE
 J. Radet, CEN/CADARACHE - Bat 506, FRANCE
 Prof. E. Economou, Univ. of Crete, GREECE
 Ms. C. Rinni, Univ. of Ioannina, GREECE
 Preprint Library, Hungarian Academy of Sci., HUNGARY
 Dr. B. DasGupta, Saha Inst. of Nuclear Physics, INDIA
 Dr. P. Kaw, Inst. for Plasma Research, INDIA
 Dr. P. Rosenau, Israel Inst. of Technology, ISRAEL
 Librarian, International Center for Theo Physics, ITALY
 Miss C. De Palo, Associazione EURATOM-ENEA , ITALY
 Dr. G. Grosso, Istituto di Fisica del Plasma, ITALY
 Prof. G. Rostangni, Istituto Gas Ionizzati Del Cnr, ITALY
 Dr. H. Yamato, Toshiba Res & Devel Center, JAPAN
 Prof. I. Kawakami, Hiroshima Univ., JAPAN
 Prof. K. Nishikawa, Hiroshima Univ., JAPAN
 Librarian, Naka Fusion Research Establishment, JAERI, JAPAN
 Director, Japan Atomic Energy Research Inst., JAPAN
 Prof. S. Itoh, Kyushu Univ., JAPAN
 Research Info. Ctr., National Instit. for Fusion Science, JAPAN
 Prof. S. Tanaka, Kyoto Univ., JAPAN
 Library, Kyoto Univ., JAPAN
 Prof. N. Inoue, Univ. of Tokyo, JAPAN
 Secretary, Plasma Section, Electrotechnical Lab., JAPAN
 S. Mori, Technical Advisor, JAERI, JAPAN
 Dr. O. Mitarai, Kumamoto Inst. of Technology, JAPAN
 Dr. G.S. Lee, Korea Basic Sci. Ctr., KOREA
 J. Hyeon-Sook, Korea Atomic Energy Research Inst., KOREA
 D.I. Choi, The Korea Adv. Inst. of Sci. & Tech., KOREA
 Prof. B.S. Liley, Univ. of Waikato, NEW ZEALAND
 Inst of Physics, Chinese Acad Sci PEOPLE'S REP. OF CHINA
 Library, Inst. of Plasma Physics, PEOPLE'S REP. OF CHINA
 Tsinghua Univ. Library, PEOPLE'S REPUBLIC OF CHINA
 Z. Li, S.W. Inst Physics, PEOPLE'S REPUBLIC OF CHINA
 Prof. J.A.C. Cabral, Instituto Superior Tecnico, PORTUGAL
 Prof. M.A. Hellberg, Univ. of Natal, S. AFRICA
 Prof. D.E. Kim, Pohang Inst. of Sci. & Tech., SO. KOREA
 Prof. C.I.E.M.A.T, Fusion Division Library, SPAIN
 Dr. L. Stenflo, Univ. of UMEA, SWEDEN
 Library, Royal Inst. of Technology, SWEDEN
 Prof. H. Wilhelmson, Chalmers Univ. of Tech., SWEDEN
 Centre Phys. Des Plasmas, Ecole Polytech, SWITZERLAND
 Bibliotheek, Inst. Voor Plasma-Fysica, THE NETHERLANDS
 Asst. Prof. Dr. S. Cakir, Middle East Tech. Univ., TURKEY
 Dr. V.A. Glukhikh, Sci. Res. Inst. Electrophys.I Apparatus, USSR
 Dr. D.D. Ryutov, Siberian Branch of Academy of Sci., USSR
 Dr. G.A. Eliseev, I.V. Kurchatov Inst., USSR
 Librarian, The Ukr.SSR Academy of Sciences, USSR
 Dr. L.M. Kovrizhnykh, Inst. of General Physics, USSR
 Kernforschungsanlage GmbH, Zentralbibliothek, W. GERMANY
 Bibliothek, Inst. Für Plasmaforschung, W. GERMANY
 Prof. K. Schindler, Ruhr-Universität Bochum, W. GERMANY
 Dr. F. Wagner, (ASDEX), Max-Planck-Institut, W. GERMANY
 Librarian, Max-Planck-Institut, W. GERMANY

DATE

FILMED

5/12/94

END